THE ASTROPHYSICAL JOURNAL SUPPLEMENT SERIES, 107:19–35, 1996 November

THE MOLONGLO REFERENCE CATALOG/1 JANSKY RADIO SOURCE SURVEY. I. RADIO GALAXY IDENTIFICATIONS

PATRICK J. MCCARTHY,[1,2,3] VIJAY K. KAPAHI,[3,4] WIL VAN BREUGEL,[3,5] S. E. PERSSON,[1]
RAMANA M. ATHREYA,[4] AND C. R. SUBRAHMANYA[4]
Received 1996 April 12; accepted 1996 June 7

ABSTRACT

This is the first in a series of papers discussing the properties of a complete set of radio sources selected near $S_{408} = 1$ Jy. We present optical or infrared identifications for a sample of 452 radio galaxies. The sources were selected from the 408 MHz Molonglo Reference Catalog, restricted only by flux density and position on the sky, as follows: $S_{408} \geq 0.95$ Jy and $-30° <$ decl. (1950) $< -20°$, and $9^h20^m <$ R.A.(1950) $< 14^h4^m$ or $20^h20^m <$ R.A.(1950) $< 6^h14^m$. This complete sample, the MRC/1 Jy survey, contains 558 radio galaxies or quasars, of which six are occulted by bright stars or galaxies and two are multiple confused sources. Of the remaining 550 sources, 527, or 96%, are identified to an r magnitude of 25, and eight additional sources are identified to $K = 19$. Of the 17 unocculted objects that remain unidentified, 15 are sources for which we have either poor radio maps or inadequate optical/IR images. This paper presents finding charts and astrometric positions for the 452 sources that are not identified as either quasars or BL Lacertae objects. Magnitudes in the r passband accurate to typically 0.1 mag are given for 353 of the radio galaxy identifications. Redshifts for 268 of the galaxies are also listed; these have been derived from 450 spectroscopic observations. The radio observations, quasar and BL Lac identifications, spectroscopy, and near-IR images will be presented in subsequent papers in this series.

Subject headings: galaxies: photometry — quasars: general — radio continuum: galaxies — surveys

1. INTRODUCTION

All studies of astronomical objects have their origins in surveys of one sort or another. Our understanding of radio galaxies and quasars in particular is strongly rooted in well-defined samples drawn from large surveys (e.g., the 3CRR; Laing, Riley, & Longair 1983). Radio surveys are also strongly motivated by their utility in identifying classes of objects that can be observed at other wavelengths, and thereby can be used for purposes beyond the study of radio source physics *per se*. The earliest radio surveys with sufficient resolution to allow the identification of the sources on optical photographs contained many sources below the limit of either the Palomar Observatory Sky Survey or the deepest prime focus plates taken at the Hale 5 m telescope (e.g., Wyndham 1966; Veron 1966). As radio observations with resolutions of several arcseconds or better became widely available (e.g., Jenkins, Pooley, & Riley 1977) it became clear that a significant fraction of strong sources could not be identified on any plate material (e.g., Kristian, Sandage, & Katem 1974; Windhorst, Koo, & Kron 1985). The use of CCDs and, more recently, near-IR arrays on large aperture telescopes allows one to identify all, or nearly all, strong and intermediate strength sources, as this paper and others demonstrate (e.g., Dunlop et al. 1989). There are, however, only a handful of radio surveys for which intensive optical follow-up observations have been made. The paucity of radio samples for which complete optical identifications and redshifts exist has hampered our ability to obtain a thorough census of the radio source population and has limited the degree to which radio sources can be used as probes of the distant universe.

This paper is the first in a series aimed at expanding our knowledge of the radio, optical, and infrared properties of a sample of sources selected solely by low-frequency flux density. This survey will be used to address a variety of astrophysical problems. Understanding the high-redshift radio galaxies and the relationship between radio galaxies and radio quasars are two examples of goals for which this program was initiated. Despite the existence of numerous radio surveys at a variety of frequencies, there are at present few complete and unbiased surveys of extragalactic sources for which corresponding optical observations are available. The 178 MHz 3CRR survey (Bennet 1962; Laing et al. 1983) is the best-studied sample of strong low-frequency selected sources and is one of the few complete radio samples for which optical identifications and redshift measurements exist for all the sources (see Rawlings et al. 1996 for the last of the 3CRR sources; see Djorgovski et al. 1988 and Spinrad et al. 1985 for the 3CR identifications). At higher frequencies there are several samples that have been fully identified with optical counterparts (e.g., Wall & Peacock 1985). The Parkes Selected Regions (Downes et al. 1986; Dunlop et al. 1989) is a large and completely identified sample selected at 2700 MHz. The redshift content for this sample, however, is fairly meager. Other high-frequency surveys having a high fraction of optical identifications and/or redshifts are confined to strong sources and sample the radio source population with a selection function

[1] The Observatories of the Carnegie Institution of Washington, 813 Santa Barbara Street, Pasadena, CA 91101; pmc2@ociw.edu, persson@ociw.edu.
[2] Hubble Fellow 1990–1993, when part of this work was performed.
[3] Guest Observer at the National Optical Astronomy Observatories, Cerro Tololo Inter-American Observatory, which is operated by the Associated Universities for Research in Astronomy, Inc., under contract with the National Science Foundation.
[4] National Centre for Radio Astrophysics, TIFR, Poona University Campus, P.O. Box 3, Ganeshkhind, Pune 411 007, India; vijay@gmrt.ernet.in, ramana@gmrt.ernet.in, crs@gmrt.ernet.in.
[5] Institute for Geophysics and Planetary Physics, LLNL, P.O. Box 808, L-413, Livermore, CA 94551; wil@igpp.llnl.gov.

strongly weighted toward self-absorbed and/or beamed sources (e.g., the sample of Pearson & Readhead 1981; the 2 Jy samples of Peacock & Wall 1981 and Wall & Peacock 1985). Ekers et al. (1989) have selected a "complete" sample of radio galaxies, but imposed an optical magnitude cutoff of $m_v = 17.0$ mag; thus their sample is not complete in the sense of this discussion (i.e., limited by radio flux density only). The identification and spectroscopy program for the Third Bologna Survey (Vigotti et al. 1989) being carried out by Djorgovski and co-workers (e.g., Thompson & Djorgovski 1994) promises to produce an additional sample with complete optical data.

Surveys at low frequency are of particular interest for finding radio galaxies, especially those at large redshifts, and in recent years several samples have become available. The low-frequency selected catalogs offer the advantage of being less affected by optical depth and beaming, and thus sample the source population with an isotropic selection criterion. The differential source counts at 408 MHz show a large excess over Euclidean predictions in the $\sim$0.25–1 Jy range of flux densities (e.g., Wall 1980; Condon 1984). Allington-Smith (1982) produced the first catalog designed to sample this rapidly evolving population of sources. The Allington-Smith sample (the B2/1 Jy), based on the Second Bologna Survey (Fanti et al. 1974 and references therein), is too small to provide much statistical leverage and remains incomplete in its redshift content. Since the time of the Allington-Smith work, a number of groups have defined other samples of sources chosen near the peak in the source counts (e.g., Eales et al. 1985a, 1985b, 1985c).

The utility of the $S_{408} \sim 1$ Jy flux limit in finding sources at high redshifts has been well demonstrated (Lilly 1988, 1989; McCarthy et al. 1990, 1991). Surveys defined by additional criteria, particularly spectral index, have been the most successful in identifying radio galaxies at high redshift, with greater efficiency than the complete flux-limited samples. The steep-spectrum samples have produced the largest number of galaxies at redshift $z > 2$ (e.g., Chambers, Miley, & van Breugel 1990; Rottgering, van Ojik, & Miley 1994; McCarthy et al. 1990, 1991; van Ojik, Miley, & Rottgering 1996; H. Spinrad et al., unpublished) and have led to the discovery of several galaxies with $z > 3$ (Chambers et al. 1990; McCarthy et al. 1990, 1991; van Ojik et al. 1996). More sophisticated selection techniques based on radio spectral shape, angular size, and flux density have led to the selection of even rarer objects, including the $z = 4.25$ radio galaxy 8C 1435+63 (Lacy et al. 1995; Spinrad, Dey, & Graham 1995). While these surveys provide an effective means of selecting distant objects, they do not necessarily give an unbiased picture of the population of radio sources at high redshift. A summary of various radio surveys relevant to high-redshift galaxies is given in McCarthy (1993).

Our expectation was that an unbiased selection of sources from a complete low-frequency catalog at a flux density near the peak of the source counts would contain a high proportion of high-redshift galaxies while still providing an unbiased sample of radio galaxies and quasars over a wide range of redshift, spectral index, and angular size. This was the primary motivation in the design of the present program, which has led to the identification of a large sample of radio sources, complete to a limiting flux density of 0.95 Jy at 408 MHz.

In addition to providing fertile ground for discovering high-redshift galaxies, the sample provides the opportunity to study properties of the radio source population itself. For example, the 3CRR, by virtue of its completeness, lends itself to statistical studies of correlations between various properties of the sources. A number of interesting correlations have been reported, viz., emission-line luminosity versus radio power (Baum & Heckman 1989; McCarthy et al. 1990; Saunders et al. 1989; Rawlings 1994), radio spectral index versus radio power (Laing & Peacock 1980), spectral index versus redshift (Chambers et al. 1990), cluster environment versus redshift (Hill & Lilly 1991; Yates, Miller, & Peacock 1989), and others. The strong Malmquist bias in the 3CRR, however, makes it often impossible to separate correlations with radio luminosity (or monochromatic power) from those with redshift. The few weaker samples that have been studied for these purposes have rarely been conclusive in breaking the degeneracy as they are small and often incomplete in their identification and redshift content (e.g., Allington-Smith et al. 1985; Owen & Keel 1995). Our program addresses these problems directly. While our limiting flux density is only a factor of $\sim$6 below that of the 3CRR [S (178 MHz) $\geq$ 10 Jy], the large number of sources provides extra leverage in breaking the redshift-power degeneracy.

This paper is the first in a series resulting from our long-term multiwavelength study of this well-defined, low-frequency, complete sample of radio sources. It is restricted to a presentation of the optical/infrared identifications, astrometry, r magnitudes, and those redshifts presently available. Kapahi et al. (1996b; hereafter Paper II) presents and discusses the VLA radio data. Kapahi et al. 1996a (hereafter Paper III) present radio data and optical identifications for the quasars and BL Lacertae objects in the sample. McCarthy, van Breugel, & Kapahi (1996b, hereafter Paper IV) presents the optical spectroscopic results. McCarthy et al. (1996a, Paper V) presents and discusses selected infrared data, optical-to-infrared energy distributions, and the K-band Hubble diagram.

2. SAMPLE DEFINITION

The Molonglo Reference Catalog (Large et al. 1981, hereafter MRC) was produced from a 408 MHz survey carried out with the Molonglo Synthesis Telescope. The limiting flux density of the MRC is 0.7 Jy, and the catalog is believed to be 99.9% complete at $S_{408} = 1$ Jy. Our sample is drawn from the MRC with the following restrictions: $S_{408} > 0.95$ Jy; $-30° <$ decl. (1950) $< -20°$, and $9^h20^m <$ R.A. (1950) $< 14^h4^m$ or $20^h20^m <$ R.A. (1950) $< 6^h14^m$. No other explicit radio (e.g., spectral index, angular size) or optical selection criteria were applied, although the survey frequency and the beam size of the Molonglo Synthesis Telescope (2.5) build in some biases in the range of spectral indices and angular sizes sampled. Our sample should be essentially complete for sources brighter than 0.95 Jy and with angular sizes less than 2.5. The sample, henceforth referred to as the MRC/1 Jy, contains 558 sources, more than 3 times the size of the 3CRR (Laing et al. 1983) and 10 times larger than the B2/1 Jy sample (Allington-Smith 1982).

The flux densities in the MRC are of high quality and precision, but the low angular resolution of the survey makes it impossible to identify more than a modest fraction ($\sim$20%) of the sources on the basis of their 408 MHz positions. Each source in the sample (with two exceptions) was imaged at 5 GHz using the VLA in its southern-source

optimized A/B or B/C configurations. A few of the largest sources were also imaged at 1400 MHz. The details of the VLA radio observations, the exact frequencies, bandwidths, and beam sizes are described in full in Paper II. The optical identifications presented here comprise only those sources not identified with either quasars or BL Lac objects and are essentially all radio galaxies. The six occulted sources and the 17 sources that remain unidentified are listed and noted herein. Many of these unidentified sources are large sources for which our maps are too poor to allow us to identify the host galaxies. Less than 1% of the sources have counterparts that are too faint to allow detection in our deep visible and near-IR imaging data.

3. OBSERVATIONS AND REDUCTIONS

3.1. *Initial Astrometry*

In order to identify all the galaxies and quasars in the radio sample we first compiled a grid of secondary astrometric stars for each field. At each VLA source position we extracted a 7.′25 × 7.′25 image from the digitized SERC J southern sky survey films at the Space Telescope Science Institute (Lasker et al. 1990). The positions of several stars were measured using GASP, the Guide Star Astrometry Software Package. The centroid of each stellar image was determined by fitting a two-dimensional Gaussian to the profile; heavily saturated stars were avoided. The 1.″7 pixels of the digitized sky survey images result in a somewhat poorer positional accuracy (rms = 1.″2, Lasker et al. 1990) than is achievable with direct measurement of the original plate material or print/film copies. The net uncertainty of ~1.″5 in the secondary plate solution derived from five to six stars did not, however, limit our ability to identify any of the sources. Approximately 25% of the radio galaxies were identified directly on the sky survey films or the digitized plates and their J2000 positions were measured therefrom. For approximately 50 of the empty field sources we measured the positions of secondary astrometric reference stars directly on the SERC J films using the two-screw Mann measuring engine located at the Carnegie offices in Pasadena. The rms uncertainty in the plate solution based on the measurement of 15–25 SAO stars was typically 0.″6–0.″9. Many of the sources identified in this manner are given in McCarthy et al. (1990, 1991).

The type of radio position that was used in searching either the plate material or the CCD images differed depending on the size and morphology of the source. For unresolved sources we fitted a two-dimensional Gaussian to the radio image to derive the position. Similarly for sources with a central component (triples and some complex sources) we fitted a Gaussian to the central component. For simple doubles we searched for identifications at the midpoint of the lobes, rather than at the centroid, although we accepted candidate identifications along the line between the lobes. Finally, for complex and marginally resolved sources, we used the centroid of the radio image as the search position. These positions are given in Table 2 of Paper II.

3.2. *CCD Imaging Observations*

Nearly all of the sources in the radio sample that were *not* identified with stellar-appearing objects on the sky survey material were imaged with either the 2.5 m du Pont or 1.0 m Swope telescopes at Las Campanas Observatory (LCO), Chile. The majority of these sources are not visible on the southern sky survey films, despite the increased depth of those films compared to the Palomar Observatory Sky Survey prints. The 2.5 m telescope was used to image all the "empty" field sources, while the 1.0 m telescope was used to image all the sources that were identified but were not clearly stellar on the SERC J sky survey. For both telescopes, the CCD imaging camera was located at the Cassegrain focus and was operated without any corrector or reimaging optics. An 800 × 800, thinned and UV-flooded, Texas Instruments CCD with 15 μm pixels was used for almost all of the imaging observations at both telescopes. A 2 × 2 pixel on-chip binning mode was used on the 2.5 m telescope, giving a scale of 0.″3317 pixel^{-1} and a field of view of 132″ × 132″. The pixel scale was determined by measuring the separations between ~900 pairs of stars whose positions had been measured on the sky survey films with the Mann engine as described above. On the 1 m telescope the TI CCD was run without binning, giving 0.″435 pixel^{-1} and a field of view of 348″ × 348″. The plate scale for the Cassegrain focus of the Swope Telescope was determined by Dr. Ian Thompson from observations of globular clusters for which accurate astrometry is available. A few observations were made at the 2.5 m telescope with either a 512 × 512 (27 μm pixels) Tektronix CCD or a 1024 × 1024 with 24 μm pixels; the scale with these devices is 0.″294 and 0.″229 pixel^{-1}, respectively. These detectors are referred to as Tek No. 1 and Tek No. 2 in Tables 1 and 2. The latter scales were determined from the known linear size of the pixels and the plate scale of the uncorrected Cassegrain focus of the 2.5 m as determined with the TI CCD.

The CCD observations were made with 2 × 2 inch *g* and *r* filters of the Thuan & Gunn (1976) photometric system, and the *i* filter of the Wade et al. (1979) system. Care was taken to use the same filters for all observations on both telescopes and over the entire 6 yr duration of the observing program. Nearly all images taken for identification purposes were in the *r* band, but in times of bright moon the *i* filter was used. Special care was taken during each run to determine the orientation of the CCD with respect to circles of constant declination. Trailed stellar images (taken with the telescope tracking off) were used to find and adjust the rotation of the CCD rows; typical residual rotations were less than 1°. Accurate knowledge of the rotation of the CCD images was crucial in determining offsets from nearby stars for subsequent spectroscopic observations. As long as the rotation was small, the astrometric solutions were robust, since the field rotation was treated as a free parameter in the fit. Curvature of the coordinate grid was a further concern, but the small size of the TI CCD and the declination of our survey ensured that this was insignificant.

The imaging observations were made during several observing runs in the period from 1989 March to 1996 January. The dates of the observing runs and a two-word summary of the prevailing conditions during each are listed in Table 1. A typical observation of a faint galaxy consisted of several exposures of 300 s duration, with the telescope offset a few arcseconds between exposures. Unless the identification was clearly visible in a single 300 s exposure, a total of 2400–2700 s of data was obtained. This provided for a reasonably uniform signal-to-noise ratio in the ensemble data set. Variations in the observing conditions from run to run, and often within a run, naturally add dispersion to the depths actually reached on the many targets. While there

TABLE 1

OBSERVING RUNS

Number	Date (UT)	Telescope (m)	Detector	Scale	Weather
1.....	1989 Mar 115	2.5	TI No. 1	0.332	Photometric
2.....	1989 Jul 29–Aug 5	2.5	TI No. 1	0.332	Poor seeing
3.....	1989 Oct 26–28	2.5	TI No. 2	0.332	Mixed
4.....	1989 Oct 29–31	2.5	TI No. 1	0.332	Mixed
5.....	1990 Apr 19–25	2.5	Tek No. 1	0.294	Lost to clouds
6.....	1990 Aug 17–19	2.5	Tek No. 1	0.294	Poor seeing
7.....	1991 Mar 10–14	2.5	TI No. 1	0.332	Mostly photometric
8.....	1991 Sep 5–9	2.5	TI No. 1	0.332	Cirrus
9.....	1992 Mar 27–31	2.5	TI No. 1	0.332	Mostly clouds
10	1992 Sep 28–Oct 1	2.5	TI No. 1	0.332	Mixed
11	1992 Oct 1–3	1.0	TI No. 1	0.435	Mostly photometric
12	1992 Oct 29–Nov 1	1.0	TI No. 1	0.435	Photometric
13	1993 Feb 18–22	2.5	TI No. 1	0.332	Mixed
14	1993 Feb 26–28	1.0	TI No. 1	0.435	Mostly photometric
15	1993 Sep 11–17	1.0	TI No. 1	0.435	Mixed
16	1993 Sep 17–22	2.5	TI No. 1	0.332	Mixed
17	1994 Mar 11–12	2.5	TI No. 1	0.332	Mixed
18	1994 Aug 29–Sep 1	2.5	TI No. 1	0.332	Mixed
19	1995 Feb 1– 3	2.5	TI No. 1	0.332	Mixed
20	1995 Sep 15–18	2.5	TI No. 1	0.332	Mixed
21	1996 Feb 17–19	2.5	Tek No. 2	0.256	Photometric

were periods of very good seeing (i.e., $\leq 1''$), many of the images taken for identification purposes were obtained in mediocre to poor seeing ($1''.2$–$1''.8$). Nearly all of the non-photometric, but still usable, nights were used to obtain images for identifications. Whenever possible the objects were reobserved for calibration purposes on a photometric night. During these nights we observed *UBVRI* standards from Landolt (1992); we used stars that have been set up as secondary *gri* standards by Thompson, Searle, & Krzeminski (1996). Standard star fields were observed several times each night at a range of airmass. The $-29°$ latitude of the observatory is such that our radio sample passes nearly overhead, and as our targets are widely distributed in right ascension it was easy to remain at airmass values of less than 1.3.

Finally, in cases where a source was visible but not clearly stellar on the sky survey, we obtained *r*- and *g*-band images using the 1.0 m telescope. These exposures were typically only 20–30 minutes in duration and were made to determine magnitudes and morphology rather than to obtain identifications.

3.3. *Optical Image Reduction*

We endeavored to obtain the maximum possible depth from the images as many of the source identifications are quite faint. For all of the *r* and *i* imaging runs on the 2.5 m telescope we constructed dark sky flat fields from a median of all the *r* or *i* images for a set of typically one to three nights' worth of data. Exposures shorter than 300 s and those containing bright stars or galaxies were not used. We found from experience that flats constructed from data obtained over two or three nights usually were satisfactory, but for longer runs more than one flat was required. Images flattened with the *r* and *i* dark sky medians were flat to 1% or better.

After each exposure was bias corrected and divided by the normalized flat field, multiple exposures of the same field were shifted into registration using a linear interpolation in each coordinate. The offsets were determined from the centroids of one to three stars in each frame. The individual frames were then summed to produce the final image, which typically reach a depth of $r \sim 25$ mag ($2\ \sigma$) for detection of an optical counterpart. In several cases scattered light from a nearby bright star significantly contaminated the region of the image near the radio source position. In these cases we removed this excess background by fitting and subtracting a low-order surface to a 200×200 pixel subsection of the image after editing out the bright stars and galaxies. This procedure is never 100% satisfactory and often leaves noticeable residuals (e.g., 1107−272, 2059−228, 2150−202). All of the optical and infrared image processing was done with NOAO's IRAF reduction package.

3.4. *Infrared Observations and Reductions*

Approximately 2% (11 sources) of the unocculted/unconfused sources in the sample remain unidentified at the $r \sim 25$ level. Eight of these sources were subsequently identified on deep *H*-band (1.5–1.8 μm), *K*-band (2.0–2.4 μm) or *K*-short (1.99–2.32 μm) images. The details of our near-infrared imaging program will be described elsewhere. Briefly, the infrared images were obtained with a 256×256 HgCdTe NICMOS3 array camera (Persson et al. 1992) mounted on the 2.5 m du Pont Telescope. For each field discussed here we took 30 or 35 s exposures and shifted the telescope a few arcseconds after every third exposure. A total of $\sim$75–120 frames were obtained for each object, giving total integration times of 2700–3600 s. Each exposure was linearized, corrected for dark counts, and then combined to make a median sky and flat-field frame. The individual exposures were sky subtracted, flattened, shifted into registration, and then combined with a mask applied to the bad pixels. The resulting images typically reach a depth of $K \sim 19.5$ mag ($2\ \sigma$) in a $4''$ diameter aperture.

3.5. *Source Identification, Astrometry, and Photometry*

Each CCD frame contains one to eight stars whose positions were determined from the sky survey material as discussed above. The centroids of these stars were measured and a secondary (CCD) frame solution was computed. From this solution we derived the pixel position of the radio

TABLE 2

OPTICAL POSITIONS OF MRC/1 Jy RADIO GALAXIES

IAU	α(1950)	δ(1950)	z	r (mag)	Filter	FOV	Run Number	Notes	Remarks
0001−233.....	00 01 29.13	−23 23 39.7	0.097	16.3	r	2	11		
0001−237.....	00 01 14.45	−23 46 24.5	0.315	18.7	r	2	11		
0006−212.....	00 06 33.01	−21 13 14.0	0.91	22.5	r	1	8, 20		
0007−287.....	00 07 26.29	−28 46 11.8	...	...	r	2	11	N	Occulted by star
0015−229.....	00 15 26.51	−22 54 43.2	2.01	23.1	r	1	10		
0017−205.....	00 18 01.51	−20 32 49.4	0.197	18.2	r	1	18		
0020−253.....	00 20 38.13	−25 19 07.0	0.35	...	i	1	18		
0022−209.....	00 22 16.66	−20 59 17	0.054	15.6	r	1	20	N	
0023−203.....	00 23 43.02	−20 21 32.9	0.845	22:	r	1	16	N	Near bright star
0023−263.....	00 23 19.04	−26 18 49.6	0.322	19.1	r	1	16		
0025−204.....	00 25 21.90	−20 24 14.0	...	...	i	1	18		
0025−277.....	00 24 59.56	−27 47 48.0	...	...	i	1	18		
0028−223.....	00 28 32.24	−22 23 42.3	0.205	18.0	r	2	11		
0029−232.....	00 29 33.66	−23 14 42.0	...	24.8	r	5	6	N	
0029−243.....	00 29 51.64	−24 21 42.3	1.29	22.5	r	1	10	N	
0030−219.....	00 30 53.86	−21 58 33.0	2.168	23.8	r	1	2		
0030−297.....	00 30 17.72	−29 47 43.0	...	23.2	r	1	18		
0032−203.....	00 32 39.07	−20 20 26.8	0.516	20.1	r	1	20		
0034−234.....	00 34 52.89	−23 25 00.2	...	22.9	r	1	4, 20		
0035−231.....	00 35 55.64	−23 09 31.9	0.685	20.6	r	1	16		
0036−216.....	00 36 00.52	−21 36 33.9	0.338	...	r	1	11		
0037−258.....	00 37 28.05	−25 50 58.2	1.100	21.5	r	5	6		
0038−209.....	00 38 18.74	−21 00 07.4	0.0906	16.5	r	2	11		
0038−294.....	00 38 44.88	−29 24 14.1	...	23.5	r	1	18		
0041−224.....	00 41 43.34	−22 28 43.2	...	...	K	3	*	N	
				>24	r	5	6		
0042−248.....	00 42 35.20	−24 50 47.8	...	21.2	r	1	16		
0045−255.....	00 45 00.00	−25 30 00	0.001	...	...	...	...	N	NGC 253
0048−233.....	00 48 25.45	−23 23 12.8	0.111	...	r	1	8	N	
0050−222.....	00 50 15.06	−22 12 02.4	0.654	19.7	r	1	20		
0052−241.....	00 52 02.91	−24 07 45.2	2.86	23.2	r	5	6	N	
0055−256.....	00 55 31.10	−25 38 48.6	0.1985	18.1	r	2	11		
0055−258.....	00 55 16.72	−25 49 26.5	...	20.4	r	2	11		
0056−242.....	00 56 01.44	−24 17 16.7	...	19.4	r	2	11		
0059−287.....	00 59 28.13	−28 47 27.3	...	22.0	r	1	18		
0100−221.....	01 00 15.09	−22 09 00.4	0.058	...	SS	4	...		
0100−277.....	01 00 19.45	−27 47 31.3	...	21.5	r	2	11		
0101−275.....	01 01 11.03	−27 31 14.7	...	22.0	r	1	18		
0102−256.....	01 02 27.14	−25 36 57.1	...	23	r	5	6	N	
0103−243.....	01 03 47.27	−24 22 40.8	...	23.5:	r	5	6		
0106−291.....	01 06 14.96	−29 07 28.0	...	...	i	1	18		
0110−224.....	01 10 03.55	−22 26 43.4	...	...	r	1	3		
0112−209.....	01 12 16.62	−20 58 41.0	...	23.2	r	1	10		
0112−219.....	01 12 51.44	−21 54 28	...	...	...	...	...	N	Not observed with VLA
0113−245.....	01 13 20.55	−24 33 04	...	...	r	1		N	Unidentified
0113−285.....	01 13 17.31	−28 32 57.2	...	22.1	r	1	18		
0114−211.....	01 14 26.00	−21 07 55.8	1.41:	22.1	r	1	18		
0115−261.....	01 15 52.65	−26 07 35.7	0.268	18.8	r	1	18	N	
0121−295.....	01 21 10.99	−29 32 08.0	...	22.4	r	1	18		
0122−255.....	01 22 23.85	−25 32 50.1	...	...	r	2	11	N	Occulted by star
0125−201.....	01 25 05.88	−20 11 42.6	...	23.5:	r	1	10		
0125−216.....	01 25 44.72	−21 37 42.0	0.340	18.7	r	1	8		
0127−276.....	01 27 48.73	−27 40 09.2	0.318	20.5:	r	2	16	N	
0128−264.....	01 28 06.59	−26 25 23.1	...	23.1	r	1	10		
0133−277.....	01 33 40.74	−27 43 02.1	...	23.8	r	5	6		
0137−263.....	01 37 32.60	−26 22 17.2	0.16:	20.1	r	1	8		
0138−218.....	01 38 49.81	−21 53 41.2	...	22.3	r	5	6		
0139−273.....	01 39 07.90	−27 21 19.4	1.44	21.4	r	1	8		
0140−257.....	01 40 21.15	−25 45 39.8	2.64	23.3	r	1	3		
0143−246.....	01 43 00.93	−24 38 35.6	0.716	21.5	r	1	20		
0144−227.....	01 44 47.96	−22 47 39.2	0.6	21.0	r	1	8		

TABLE 2—*Continued*

IAU	α(1950)	δ(1950)	*z*	*r* (mag)	Filter	FOV	Run Number	Notes	Remarks
0146−224.....	01 46 52.64	−22 26 30.9	0.36	19.3	*r*	2	11		
0147−288.....	01 47 13.05	−28 53 17.6	...	22.3	*r*	1	18		
0148−297.....	01 48 19.59	−29 46 46.3	0.41	21.3	*r*	2	11		
0149−260A.....	01 49 34.9	−26 02 11.0	0.144	17.2	*r*	2	11	N	East source
0149−260B.....	01 49 32.03	−26 02 06.4	...	19.6	*r*	2	11		West source, galaxy B1
0149−299.....	01 49 44.83	−29 55 47.4	0.6034	20.7	*r*	1	20		
0150−275.....	01 50 05.92	−27 33 42.4	...	21.2	*r*	1	16		
0152−209.....	01 52 34.05	−20 55 08.3	1.89	21.9	*r*	7	*		
0152−260.....	01 52 32.22	−26 03 02.6	...	20.4	*r*	5	6		
0155−212.....	01 55 32.12	−21 16 54.5	0.159	17.0	*r*	2	11		
0155−225.....	01 55 54.21	−22 35 16.6	...	22.7	*r*	1	18		
0156−252.....	01 56 15.05	−25 14 04.0	2.09	22.9	*r*	1	2		
0156−278.....	01 56 36.64	−27 50 40.9	0.33	19.0	*r*	2	11		
0201−214.....	02 01 11.61	−21 28 11.0	0.915	21.3	*r*	1	10		
0203−209.....	02 03 16.61	−20 57 07.1	1.257	22.8:	*r*	1	2	N	
0205−223.....	02 05 27.98	−22 18 59.6	...	22.6	*r*	1	18		
0205−229.....	02 05 20.34	−22 59 12.3	0.68	20.6	*r*	1	18		
0208−240.....	02 08 59.68	−24 05 29.5	0.23	18.2	*r*	2	11		
0209−282.....	02 09 55.81	−28 14 14.7	0.6	21.2	*r*	1	16		
0211−256.....	02 11 14.24	−25 39 19.3	1.30	21.6	*r*	1	16		
0211−258.....	02 11 34.89	−25 52 37.3	...	21.3	*r*	1	20	N	
0216−250.....	02 16 27.82	−25 01 58.8	...	22.1	*r*	1	20		
0221−285.....	02 21 31.07	−28 32 32.3	...	18.9	*r*	1	20	N	Uncertain ID
0223−245.....	02 23 13.74	−24 34 45.3	0.634	21.4	*r*	1	16		
0225−241.....	02 25 17.56	−24 08 21.1	0.52	19.5	*r*	1	20		
0226−284A.....	02 26 17.06	−28 27 02.2	0.21	17.4	*r*	1	18	N	
0226−284B.....	02 26 11.67	−28 28 10.0	...	17.5	*r*	1	18		
0226−292.....	02 26 03.07	−29 18 01.9	...	24.1:	*r*	1	10		
0229−208.....	02 29 18.66	−20 53 36.3	0.087	16.2	*r*	1	8		
0230−245.....	02 30 15.31	−24 35 17.2	0.88	19.4	*r*	1	8		
0231−235.....	02 31 08.84	−23 34 12.9	0.81	21.5:	*r*	1	20		
0233−290.....	02 33 45.74	−29 03 50.2	0.725	22.2	*r*	2	11		
0237−201.....	02 37 19.47	−20 06 18.8	1.03	23.2	*r*	1	8		
0240−217.....	02 40 19.37	−21 45 08.3	0.314	...	*r*	1	20		
0242−221.....	02 42 08.85	−22 06 23.0	...	...	*K*	3	*	N	
			...	...	*r*	1	10		
0245−263.....	02 45 35.01	−26 21 46.7	0.35	19.6	*r*	2	16		
0245−297.....	02 45 49.66	−29 43 42.6	0.36	18.9	*r*	1	18		
0246−202.....	02 46 43.74	−20 14 57.2	0.58	20.9	*r*	1	11		
0247−205.....	02 47 09.49	−20 35 45.2	0.32	...	*r*	2	11		
0247−207.....	02 47 17.29	−20 42 59.1	0.085	15.6	*r*	2	16		
0251−273.....	02 51 06.45	−27 21 22.2	3.16	23.0	*r*	1	16	N	
0252−246.....	02 52 42.97	−24 39 56.3	1.30	23.4:	*r*	1	10		
0253−206.....	02 53 35.34	−20 39 51.6	0.69	...	*r*	1	8		
0253−220.....	02 53 24.02	−22 05 59.6	0.112	16.6	*r*	2	11		
0253−259.....	02 53 33.07	−25 59 45.2	...	...	*r*	1	8		
0254−236.....	02 54 01.25	−23 36 58.4	0.509	20.0	*r*	1	16		
0254−263.....	02 54 06.11	−26 22 37.4	0.31	...	*r*	1	8		
0254−274.....	02 54 41.80	−27 29 59.6	0.48	19.2	*r*	5	6		
0255−247.....	02 55 15.6	−24 45 46	...	...	*r*	1	16	N	Unidentified
0255−262.....	02 55 28.80	−26 12 12.0	0.36	19.9	*r*	1	8		
0256−236.....	02 56 38.36	−23 41 46	...	...	SS	4	...	N	Unidentified
0259−252A.....	02 59 03.89	−25 17 30	...	...	SS	7	...	N	Unidentified
0259−252B.....	02 59 16.05	−25 15 39	...	...	...	...	...		Unidentified
0302−273.....	03 02 12.50	−27 22 44.9	0.115	17.3	*r*	2	11		
0305−226.....	03 05 17.73	−22 36 44.1	0.268	18.3	*r*	1	16		
0305−246.....	03 05 26.36	−24 41 22.7	1.265	22.0	*r*	2	10		
0309−260.....	03 09 37.76	−26 04 34.5	...	23.1	*r*	1	16	N	
0312−271.....	03 12 35.5	−27 11 06	...	...	*r*	2	11	N	Unidentified; multiple sources
0313−271.....	03 13 56.20	−27 09 17.3	0.216	17.7	*r*	2	11		
0315−205.....	03 15 50.11	−20 31 10.9	...	20.7	*r*	1	10	N	

TABLE 2—*Continued*

IAU	α(1950)	δ(1950)	z	r (mag)	Filter	FOV	Run Number	Notes	Remarks
0316−257.....	03 16 02.66	−25 46 03.7	3.13	22.6	*r*	1	2	N	
0319−298.....	03 19 24.32	−29 51 29.2	0.583	19.5	*r*	2	11		
0320−263.....	03 20 56.61	−26 20 22.1	...	20.7	*r*	1	20		
0320−267.....	03 20 53.13	−26 46 52.0	0.9:	22.5	*r*	1	8		
0324−228.....	03 24 52.62	−22 50 06.7	1.89	23.8	*r*	1	3		
0325−260.....	03 25 33.18	−26 02 21.1	0.638	21.2	*r*	1	3, 20		
0326−288.....	03 26 31.60	−28 52 15.3	0.108	16.8	*r*	1	8		
0327−261.....	03 27 03.50	−26 10 38	...	...	*r*	1	13	N	Unidentified; multiple sources
0337−216.....	03 37 26.88	−21 39 04.9	0.414	19.2	*r*	2	16		
0344−291.....	03 44 58.98	−29 09 40.9	0.137	17.0	*r*	1	8		
0345−206.....	03 45 41.65	−20 36 42.1	...	21.4	*r*	1	10		
0346−297.....	03 46 07.71	−29 42 10.9	0.413	20.3	*r*	1	19		
0346−298.....	03 46 49.76	−29 53 00.0	...	23.0	*r*	1	3		
0349−211.....	03 48 59.76	−21 06 58.5	2.31	24.5	*r*	1	8		
0349−278.....	03 49 31.66	−27 53 30.9	0.066	16.8	*r*	1	16	N	
0350−279.....	03 50 47.88	−27 58 12.9	1.90	24.6	*r*	1	13		
0353−207.....	03 53 25.60	−20 42 06	...	...	*r*	1	8	N	Unidentified
0354−263.....	03 54 46.15	−26 21 21.4	...	17.7	*r*	1	19		
0357−247.....	03 57 49.19	−24 42 21.8	0.205	17.8	*r*	2	11		
0357−264.....	03 57 28.43	−26 23 59	...	...	*r*	2	11	N	Unidentified
0359−294.....	03 59 20.45	−29 29 45.7	...	21.7	*r*	1	8		
0400−247.....	04 00 41.80	−24 46 15.4	1.105	21.8	*r*	1	8, 20		
0406−244.....	04 06 44.41	−24 26 08.1	2.44	22.7	*r*	1	3		
0412−204.....	04 12 56.86	−20 29 40.1	0.69	21.6	*r*	1	10		
0415−221.....	04 15 46.02	−22 08 03.7	...	22.4:	*r*	1	13		
0420−263.....	04 20 30.47	−26 23 40.8	0.131	...	SS	4	...		
0422−249.....	04 22 56.88	−24 58 18.2	...	...	*K*	3	*	N	
			...	>24	*r*	1	10		
0424−268.....	04 24 37.83	−26 50 27.0	0.47	19.9	*r*	1	13		
0428−236.....	04 28 58.48	−23 38 18	...	...	*r*	2	11	N	Unidentified
0428−271.....	04 28 16.34	−27 06 21.4	0.84	21.7	*r*	1	15, 20		
0428−281.....	04 28 16.98	−28 07 12.4	0.65	20.8	*r*	1	10	N	
0429−267.....	04 29 56.88	−26 44 30.2	1.27	22.1	*r*	1	3		
0430−235.....	04 30 45.81	−23 30 47.3	0.82	20.7	*r*	1	19		
0431−250.....	04 31 53.47	−25 01 46	...	>24	*r*	1	19	N	Unidentified
0431−292.....	04 31 36.52	−29 12 15.0	0.406	...	*r*	1	3		
0434−225.....	04 34 27.34	−22 32 37.5	0.067	15.6	*r*	2	11		
0436−203.....	04 36 32.96	−20 25 08	...	...	...	...	...	N	Unidentified
0436−294.....	04 36 33.03	−29 25 08.4	0.808	21.5	*r*	1	13		
0437−253.....	04 37 50.23	−25 18 52.6	...	20.8	*r*	1	19		
0442−282.....	04 42 37.70	−28 15 23.8	0.147	17.2	*r*	2	11		
0442−285.....	04 42 27.86	−28 32 37.8	...	24.2	*r*	1	19		
0442−289.....	04 42 45.37	−28 57 11	...	...	...	...	...	N	Unidentified
0445−221.....	04 45 29.25	−22 08 51.5	...	...	*r*	1	10		
0446−206.....	04 46 20.54	−20 37 37.8	0.074	16.2	*r*	2	11		
0450−288.....	04 50 36.93	−28 51 37.0	...	...	*K*	3	*		
0452−260.....	04 52 31.20	−26 02 46.5	0.141	16.9	*r*	2	11		
0453−206.....	04 53 14.01	−20 38 57.3	0.035	15.1	*r*	2	11		
0457−235.....	04 57 11.52	−23 35 21.0	1.96	...	*r*	1	19	N	
0457−247.....	04 57 51.04	−24 44 04.3	0.186	17.4	*r*	2	11		
0458−208.....	04 58 21.52	−20 51 43.7	...	...	*r*	1	13		
0503−284.....	05 03 38.01	−28 28 16.5	0.037	16.4	*r*	1	18		
0508−220.....	05 08 53.11	−22 05 31.6	0.16	17.5	*r*	1	19		
0512−200.....	05 12 42.63	−20 00 41.5	0.133	16.8	*r*	2	11		
0516−275.....	05 16 22.02	−27 33 54.5	...	21.9	*r*	1	19		
0519−208.....	05 19 30.14	−20 50 31.0	...	...	*r*	1	3		
0520−289.....	05 20 03.40	−28 58 58.5	0.068	...	SS	4	...		
0522−239.....	05 22 49.68	−23 54 56.9	0.5	19.3	*r*	1	7		
0522−263.....	05 22 08.33	−26 22 55.5	0.29	...	SS	4	...		
0524−234.....	05 24 29.84	−23 28 39.4	...	23.3	*r*	1	13		

TABLE 2—*Continued*

IAU	α(1950)	δ(1950)	z	r (mag)	Filter	FOV	Run Number	Notes	Remarks
0527−255.....	05 27 19.40	−25 31 01.0	...	21.9	r	1	7		
0528−212.....	05 28 35.45	−21 15 13.9	...	24.0:	r	1	13		
0529−210.....	05 29 41.23	−21 01 38.3	0.42	18.4	r	1	19		
0531−237.....	05 31 50.07	−23 46 28.2	0.851	21.2	r	1	7		
0541−243.....	05 41 03.83	−24 22 18.9	0.523	20.1	r	1	19		
0541−288.....	05 41 24.48	−28 53 52.5	...	...	K	3	*	N	
0543−265.....	05 43 57.68	−26 31 17.9	0.85	20.9	r	1	7	N	
0551−226.....	05 51 17.26	−22 40 17.7	...	21.0	r	1	13	N	
0552−249.....	05 52 21.63	−24 56 13.8	...	23.5:	r	1	19	N	
0555−229.....	05 55 00.54	−22 55 25.2	...	23.1	r	1	19		
0556−281.....	05 56 22.40	−28 09 24.5	...	...	r	1	13		
0556−289.....	05 56 02.99	−28 56 00.1	...	20.0	r	1	19		
0557−235.....	05 57 03.02	−23 30 51.2	...	...	K	3	*	N	
0600−219.....	06 00 10.48	−21 58 16.0	1.71	24.5	r	1	17		
0602−289.....	06 02 08.46	−28 58 36.5	0.56	21.3	r	1	14		
0614−295.....	06 14 45.84	−29 30 03.6	...	...	K	3	*	N	
0930−200.....	09 30 26.99	−20 04 34.9	0.769	21.2	r	1	13		
0937−250.....	09 37 24.32	−25 02 35.6	...	20.8	r	1	13		
0938−205.....	09 38 30.99	−20 33 46.5	0.371	20.2	r	2	14		
0943−242.....	09 43 15.93	−24 14 57.8	2.93	22.3	r	1	1		
0946−237.....	09 46 12.59	−23 42 42.3	...	22.0	r	1	13	N	
0946−262.....	09 46 53.02	−26 16 29.8	...	...	K	3	*	N	
0947−217.....	09 47 34.0	−21 42 25	...	...	r	1	1	N	Unidentified
0947−249.....	09 47 36.01	−24 57 44.5	0.854	21.6	r	1	19	N	
0949−206.....	09 49 09.17	−20 36 25.4	1.158	22.9	r	1	13		
0950−239.....	09 50 53.96	−23 58 16.0	...	19.3	r	2	14		
0952−224.....	09 52 20.48	−22 27 02.8	0.228	18.0	r	1	7		
0955−283.....	09 55 36.53	−28 23 47.5	...	21.1	r	2	14	N	
0955−288.....	09 55 49.99	−28 49 46.3	1.406	21.8	r	1	13		
0956−256.....	09 56 06.09	−25 41 53.3	...	22.8	r	1	7		
0958−227.....	09 58 26.19	−22 45 21.0	0.700	...	r	1	13	N	
0959−225.....	09 59 37.42	−22 32 20.2	0.895	21.1	r	2	14		
0959−236.....	09 59 53.32	−23 40 59.0	...	22.6	r	1	13		
0959−263.....	09 59 06.66	−26 22 55.1	0.677	19.6	r	1	1		
1002−215.....	10 02 50.28	−21 30 16.0	0.59	20.5	r	1	1		
1002−216.....	10 02 47.31	−21 37 47.0	0.49	20.4	r	1	14		
1006−214.....	10 06 12.94	−21 24 28.5	0.246	18.2	r	1	1		
1006−286.....	10 06 54.40	−28 41 08.8	0.582	20.7	r	1	13	N	
1008−233.....	10 08 28.78	−23 22 37.3	1.18	21.4	r	1	7		
1009−259.....	10 09 35.17	−25 55 23.4	...	20.9	r	1	19		
1012−237.....	10 12 43.04	−23 42 18.2	0.993	...	r	1	9		
1014−200.....	10 14 46.86	−20 01 43.4	...	22.2	r	1	13		
1014−278.....	10 14 46.43	−27 49 06	...	...	r	1	9	N	Unidentified
1017−220.....	10 17 26.92	−22 04 53.7	1.768	21.6	r	2	14		
1021−217.....	10 21 22.95	−21 43 14.9	...	22.8	r	1	1	N	
1022−241.....	10 22 44.33	−24 10 57.7	...	...	r	1	9		
1022−250.....	10 22 57.09	−25 01 10.1	0.34	19.3	r	2	14		
1022−299.....	10 22 11.66	−29 57 49.6	0.911	...	r	1	9		
1023−226.....	10 23 10.31	−22 38 06.4	0.586	20.6	r	1	14	N	
1023−243.....	10 23 12.30	−24 20 56	...	...	H	3	*	N	
1025−270.....	10 25 37.47	−27 01 50.4	0.72	21.2	r	2	14		
1025−293.....	10 25 44.55	−29 21 54.5	...	...	r	1	1		
1026−202.....	10 26 35.21	−20 12 03.0	0.566	21.3:	r	1	13		
1027−225.....	10 27 20.78	−22 33 02.9	0.15:	23.1	r	1	19	N	
1029−233.....	10 29 12.23	−23 23 55.4	0.611	20.4	r	1	13		
1033−251.....	10 33 49.67	−25 09 37.6	0.44	19.9	r	1	13		
1033−259.....	10 33 56.24	−25 57 13.1	...	...	SS	4	...		
1034−265.....	10 34 48.4	−26 32 07	...	...	r	1	13	N	Occulted by star
1035−288.....	10 35 03.32	−28 52 17.7	1.276	22.5	r	1	13		
1036−215.....	10 36 17.41	−21 35 28.9	0.585	20.0	r	1	1		

TABLE 2—*Continued*

IAU	α(1950)	δ(1950)	z	r (mag)	Filter	FOV	Run Number	Notes	Remarks
1040−285.....	10 40 33.64	−28 33 34.6	1.63	...	J	3	*	N	
1043−216.....	10 43 05.50	−21 37 53.5	1.105	...	r	1	1		
1048−211.....	10 48 35.40	−21 07 20	...	>24	r	1	1	N	Unidentified
1048−238.....	10 48 09.78	−23 50 01.0	0.206	...	K	3	*		
1048−272.....	10 48 19.04	−27 17 12.3	1.558	21.3	r	1	7		
1049−201.....	10 49 05.63	−20 07 51.1	1.116	23.5	i	1	13		
1051−274.....	10 51 57.47	−27 28 50.0	...	23.0	r	1	1	N	Two possible IDs
	10 51 56.92	−27 28 49.8		...	K	3			
1053−282.....	10 53 09.75	−28 15 31.2	0.061	...	SS	4	—		
1056−272.....	10 56 32.10	−27 14 25.1	0.25	17.8	r	1	1		
1103−208.....	11 03 54.36	−20 52 47.1	1.12	21.4	r	1	13		
1103−244.....	11 03 45.73	−24 28 28.9	0.05	17.2	r	1	1		
1106−258.....	11 06 03.99	−25 48 49.6	2.43	21.2	r	1	1		
1107−218.....	11 07 44.97	−21 51 11.8	...	22.8	r	1	13		
1107−227.....	11 07 21.11	−22 46 12.7	...	...	r	1	19		
1107−272.....	11 07 41.75	−27 13 46.	...	...	r	1	13	N	No map
1108−212.....	11 08 53.36	−21 12 27.2	...	...	r	1	9	N	
1110−217.....	11 10 21.68	−21 42 09.8	...	...	r	1	9		
1112−239.....	11 12 09.26	−23 56 03.1	1.538	...	r	1	1		
1114−217.....	11 14 45.87	−21 46 38.1	...	22.4	r	1	13		
1117−217.....	11 17 41.18	−21 43 26.7	...	...	K	3	*	N	
1126−246.....	11 26 34.55	−24 41 09.2	0.155	17.0	r	2	14		
1126−258.....	11 26 32.19	−25 53 51.6	0.979	22.1	r	1	1		
1126−290.....	11 26 25.72	−29 05 01.7	0.41	19.1	r	2	14		
1128−268.....	11 28 34.44	−26 48 43.6	1.43	21.3	i	1	7		
1129−250.....	11 29 12.60	−25 03 53.5	1.065	22.7	r	1	1		
1131−269.....	11 31 01.85	−26 58 46.0	1.711	23.5:	r	1	1		
1132−258.....	11 32 11.72	−25 52 35.8	...	...	SS	4	...	N	
1136−211.....	11 36 22.48	−21 07 07.2	0.87	21.2	r	1	13	N	
1137−257.....	11 37 55.16	−25 46 16.7	...	...	i	1	13	N	
1138−262.....	11 38 17.45	−26 12 31.7	2.17	21.4	r	1	1, 7	N	
1139−285.....	11 39 03.61	−28 34 09.7	0.85	...	r	1	9		
1142−206.....	11 42 22.39	−20 40 43.8	...	...	V	6	21		
1142−242.....	11 42 45.83	−24 15 38.8	...	...	r	1	9		
1145−248.....	11 45 04.16	−24 48 07.0	...	23.1	r	2	14	N	
1152−204.....	11 52 00.54	−20 28 06.2	...	...	r	1	9		
1153−231.....	11 53 36.22	−23 10 34.5	...	18.2	r	2	14		
1155−214.....	11 55 40.74	−21 29 38.9	...	...	r	1	13		
1158−275.....	11 58 36.10	−27 33 20.8	...	...	K	3	*		
1210−290.....	12 10 14.16	−29 00 08.9	...	...	K	3	*	N	
			...	>24	r	1	7		
1211−259.....	12 11 08.10	−25 57 05.4	...	...	r	1	9		
1211−272.....	12 11 48.79	−27 14 09.2	1.893	24.5	r	1	13		
1212−204.....	12 12 09.59	−20 24 14.3	...	22.2	r	1	19		
1215−215.....	12 15 09.08	−21 30 47.3	0.072	17.7	r	2	14		
1217−276.....	12 17 45.79	−27 36 24.7	1.899	23.6	r	1	13		
1219−264.....	12 19 03.45	−26 29 37.4	...	23.0	r	1	13, 19	N	
1222−252.....	12 22 13.73	−25 12 07.5	0.077	...	SS	4	—		
1224−208.....	12 24 55.22	−20 48 37.9	...	22.5	r	1	13		
1226−211.....	12 26 08.80	−21 09 40.8	0.1913	18.8	r	2	14		
1230−244.....	12 30 05.22	−24 29 19.0	0.257	...	K	3	*		
1235−226.....	12 35 33.14	−22 39 37.2	0.778	21.0	r	1	19		
1236−200.....	12 36 54.53	−20 05 30.9	...	23.7	r	1	19		
1238−236.....	12 38 12.80	−23 38 00.4	0.9	22.0	r	1	9		
1239−256.....	12 39 55.01	−25 42 00.7	...	...	i	1	7	N	
1240−209.....	12 40 33.86	−20 55 49.2	0.42	19.5	r	1	7		
1240−271.....	12 40 16.93	−27 09 46.4	...	22.7	r	1	7, 19		
1241−275.....	12 41 10.18	−27 35 54.5	...	...	SS	4	...		
1241−291.....	12 41 24.02	−29 08 25.5	...	...	r	1	9		
1245−292.....	12 45 58.89	−29 15 35.0	...	23.5:	r	1	13	N	

TABLE 2—*Continued*

IAU	α(1950)	δ(1950)	z	r (mag)	Filter	FOV	Run Number	Notes	Remarks
1246−206.....	12 46 42.21	−20 38 52.8	...	20.3	r	2	14		
1246−231.....	12 46 25.41	−23 08 01.2	0.68	21.5	r	1	7		
1251−289.....	12 51 58.73	−28 57 24.7	0.058	...	SS	4	—		
1254−268.....	12 54 47.25	−26 51 33.1	0.135	17.1	r	2	14		
1255−282.....	12 55 42.00	−28 13 04.5	...	...	r	2	14	N	Possible QSO
1257−253.....	12 57 07.16	−25 23 28.9	0.06	...	SS	4	—		
1258−211.....	12 58 11.27	−21 10 14.0	1.58	...	i	1	7	N	
1258−229.....	12 58 17.48	−22 56 07.5	0.127	16.3	r	2	14		
1259−200.....	12 59 12.58	−20 04 33.9	1.58	...	r	1	13		
1302−206.....	13 02 58.92	−20 39 17.2	...	>20	r	1	13	N	
1303−215.....	13 04 00.87	−21 31 49.6	0.12	17.4	r	2	14		
1306−262.....	13 06 33.19	−26 18 01.4	...	20.3	r	1	19		
1307−217.....	13 07 36.71	−21 43 41.8	...	...	r	1	9	N	
1308−220.....	13 08 57.33	−22 00 45.4	0.8	...	r	1	13		
1309−201.....	13 09 26.56	−20 10 58.5	...	...	i	1	13		
1309−211.....	13 09 09.77	−21 06 41.5	0.3	19.1	r	2	14		
1309−294.....	13 09 38.50	−29 24 39.4	0.67	20.1	r	1	7		
1312−274.....	13 12 32.75	−27 29 19.6	...	22.5:	r	2	14		
1313−248.....	13 13 27.94	−24 50 45.8	0.74:	20.8	r	1	13		
1313−267.....	13 13 18.96	−26 42 30.0	...	22.0	r	1	7, 19		
1323−271.....	13 23 24.38	−27 10 03.4	0.044	...	SS	4	...		
1324−262.....	13 24 08.84	−26 16 09.2	2.28	23.3	r	1	7		
1325−222.....	13 25 53.83	−22 16 02.9	0.4	19.4	r	1	13		
1325−257.....	13 25 54.69	−25 42 28.9	0.62	20.7	r	2	14		
1328−257.....	13 28 22.50	−25 44 19.8	...	19.8	r	1	13		
1329−257.....	13 29 45.77	−25 44 21.3	0.19	18.1	r	2	14		
1331−214.....	13 31 24.92	−21 27 59.6	...	23.8	r	1	1		
1334−296.....	13 34 10.00	−29 36 37	0.001	...	...	...	...	N	NGC 5236
1336−276.....	13 36 37.80	−27 39 56.1	...	23.0:	r	1	13		
1343−253.....	13 43 55.56	−25 22 37.8	0.129	...	r	1	7	N	
1344−216.....	13 44 45.96	−21 41 50.9	0.33	18.3	r	2	14		
1344−241.....	13 44 25.02	−24 07 22.8	0.019	...	SS	4	—		
1346−252.....	13 46 05.22	−25 12 27.4	0.125	16.6	r	1	13		
1347−218.....	13 47 28.02	−21 49 50.9	...	21.4	r	1	9		
1351−235.....	13 51 02.4	−23 35 48	...	>24	r	1	13	N	Unidentified
1353−216.....	13 53 28.27	−21 37 58.9	...	22.9	r	1	1		
1353−245.....	13 53 13.01	−24 33 42.4	...	...	SS	4	...		
1354−251.....	13 54 27.24	−25 08 49.1	0.037	...	SS	4	...		
1357−217.....	13 57 08.76	−21 42 06.2	...	...	i	1	13		
1358−214.....	13 58 47.27	−21 27 41.3	0.50	20.5	r	1	1		
1401−296.....	14 01 27.72	−29 37 42.8	...	...	r	1	13		
1402−253.....	14 02 08.91	−25 21 18.1	0.74	20.2	r	1	7, 9		
2020−211.....	20 20 04.40	−21 06 39.0	0.054	16.2	r	2	11		
2025−218.....	20 25 04.29	−21 50 54.0	2.63	22.1	r	1	8		
2028−223.....	20 28 00.00	−22 21 00	...	...	—	1	—	N	No map
2028−293.....	20 28 19.64	−29 21 44.1	0.498	20.1	r	1	18		
2036−254.....	20 36 26.30	−25 25 08.0	2.0	23.5:	r	1	16	N	Near galaxy
2038−280.....	20 38 42.83	−28 03 36.1	0.39	19.8	r	1	2		
2039−236.....	20 39 20.46	−23 40 55.4	0.621	20.8	r	1	4, 16		
2039−291.....	20 39 36.85	−29 06 24.7	...	23.9	r	1	8	N	
2040−219.....	20 40 20.42	−21 55 23.6	0.204	19.4	r	1	8		
2040−267.....	20 40 46.44	−26 43 52.7	0.04	14.9	r	1	8		
2042−293.....	20 42 56.62	−29 18 47.4	...	23.0	r	1	10		
2044−272.....	20 44 18.51	−27 13 41.3	...	>24.4	r	1	8	N	Tentative ID
2045−245.....	20 45 17.39	−24 31 43.8	0.73	22.3	i	1	11, 18		
2045−256.....	20 45 43.68	−25 38 05.3	...	...	r	1	20	N	
2045−260.....	20 45 35.38	−26 03 48.6	...	22.5	r	1	20		
2048−272.....	20 48 04.29	−27 14 20.4	2.06	...	K	3	*	N	
				>24	r	1	12		
2052−253.....	20 52 04.77	−25 21 21.4	2.6	23.8	r	1	16		

TABLE 2—*Continued*

IAU	α(1950)	δ(1950)	z	r (mag)	Filter	FOV	Run Number	Notes	Remarks
2053−201.....	20 53 12.98	−20 08 08.1	0.155	17.3	*r*	1	18		
2057−286.....	20 57 12.77	−28 40 47.1	0.605	21.2	*r*	1	10	N	
2058−237.....	20 58 43.86	−23 45 26.6	...	25:	*r*	1	8	N	
					K	3	*		
2058−282.....	20 58 38.76	−28 13 45.4	0.038	15.3	*r*	2	2		
2059−228.....	20 59 00.75	−22 48 38.5	...	22.4	*r*	1	2		
2100−280.....	21 00 37.71	−28 01 15.7	...	23.2	*r*	1	20		
2101−214.....	21 01 25.73	−21 25 01.0	0.198	17.0	i	1	16		
2104−242.....	21 04 03.68	−24 17 16.9	2.49	22.7	*r*	1	3		
2104−256.....	21 04 29.90	−25 37 48.5	0.037	15.1	*r*	2	11		
2104−290.....	21 04 01.34	−29 02 53.6	...	>24	*r*	1	10	N	
			...	...	*K*	3	*		
2105−238.....	21 05 40.25	−23 49 24.4	...	23.5	i	1	16		
2107−285.....	21 07 33.30	−28 30 21.1	...	20.7	i	1	18		
2111−275.....	21 11 34.02	−27 30 13.7	...	...	*r*	1	6	N	
				...	*K*	3	*		
2113−211.....	21 13 45.42	−21 08 16.8	0.698	21.5	*r*	1	16		
2115−253.....	21 15 01.09	−25 19 11.2	1.114	22.0	*r*	1	2		
2116−250.....	21 16 08.36	−25 04 53.0	0.467	17.3	*r*	2	16		
2116−294.....	21 16 29.5	−29 23 17	...	...	*r*	1	2	N	Unidentified
2117−269.....	21 17 49.07	−26 57 25.5	0.103	18.4	*r*	2	11		
2118−266.....	21 18 23.12	−26 41 41.8	0.343	18.9	*r*	2	16		
2118−296.....	21 18 14.01	−29 39 27.2	...	22.6:	*r*	1	16		
2123−292.....	21 23 43.07	−29 14 06.6	...	...	*r*	1	8	N	
2125−237.....	21 25 13.71	−23 42 50.8	0.95	21.2	*r*	1	18		
2126−230.....	21 26 46.75	−23 01 33.7	...	23.2	*r*	1	10		
2131−241.....	21 31 46.32	−24 09 01.8	...	20.3	*r*	1	20	N	
2132−236.....	21 32 23.46	−23 35 59.3	0.81	22.4	*r*	1	15		
2134−281.....	21 34 18.90	−28 08 22.8	0.07	17.4	*r*	2	11		
2135−209.....	21 35 01.35	−20 56 04.0	0.635	19.9	*r*	2	11		
2135−257.....	21 35 08.64	−25 45 21.0	1.31:	23.7	*r*	1	8		
2136−261.....	21 36 32.12	−26 10 22.2	...	24.2:	*r*	1	8, 20		
2137−279.....	21 37 20.48	−27 59 42.7	0.64:	21.3	*r*	1	10, 16		
2139−292.....	21 39 21.66	−29 12 21.5	2.55	21.2	*r*	1	8		
2144−236.....	21 44 50.99	−23 37 37.9	...	23.4	*r*	1	18		
2144−279.....	21 44 38.30	−27 56 25.0	...	22.8	*r*	1	16		
2148−228.....	21 48 27.73	−22 50 53.9	0.85	21.8	*r*	1	18		
2149−287.....	21 49 10.64	−28 42 36.9	0.479	21.2	*r*	2	11		
2150−202.....	21 50 56.18	−20 15 21.5	...	21.5:	*r*	1	20		
2151−283.....	21 51 56.78	−28 22 40	...	—	*r*	1	16		Unidentified
2154−293.....	21 54 13.21	−29 21 58.0	0.63	20.5	*r*	1	8		
2155−255.....	21 55 21.26	−25 30 21.0	...	23.5	i	1	18		
2159−201.....	21 59 56.20	−20 09 39.9	...	23.9	*r*	1	20		
2200−251.....	22 00 04.68	−25 06 27.3	...	23.6:	*r*	1	2		
2201−272.....	22 01 44.74	−27 15 53.4	0.93:	22.2	*r*	1	8		
2204−202.....	22 04 30.59	−20 18 08.0	1.61	21.6	*r*	1	12		
2206−237.....	22 06 32.67	−23 46 41.1	0.087	16.6	*r*	2	11		
2206−251.....	22 06 34.55	−25 08 16.8	0.158	18.0	*r*	2	11		
2210−283.....	22 10 46.83	−28 18 41.2	...	20.5	*r*	1	16		
2211−252.....	22 11 41.36	−25 16 22.5	...	23.4	*r*	1	20		
2216−206.....	22 16 59.80	−20 36 33.7	1.148	22.1	*r*	1	20		
2216−281.....	22 16 53.51	−28 11 33.0	0.657	21.4:	*r*	1	20		
2217−251.....	22 17 50.56	−25 09 08.4	...	23.4	*r*	1	20		
2222−277.....	22 22 28.67	−27 42 30.6	...	22.2	*r*	1	8, 18		
2224−273.....	22 24 55.80	−27 20 21.1	1.68	22.5	*r*	1	16		
2226−224.....	22 26 59.13	−22 26 08.5	0.38	18.9	*r*	1	18		
2226−297.....	22 26 29.05	−29 47 06.2	0.73	21.3	*r*	1	16		
2229−228.....	22 29 21.40	−22 49 07.7	0.542	...	*r*	1	20		
2230−206.....	22 30 42.12	−20 40 23.7	0.6	20.8	*r*	1	8		
2232−232.....	22 32 35.81	−23 15 21.8	0.87	21.8	*r*	1	8		
2236−264.....	22 36 34.32	−26 25 46.8	0.43	19.2	*r*	2	11		

TABLE 2—*Continued*

IAU	α(1950)	δ(1950)	z	r (mag)	Filter	FOV	Run Number	Notes	Remarks
2238−216.....	22 38 45.90	−21 36 20.0	0.401	...	r	1	20		
2247−232.....	22 47 47.09	−23 17 04.9	1.33	24.4:	r	1	3	N	
					K	3	*		
2247−248.....	22 47 03.47	−24 50 43.3	1.63	22.5	r	1	2		
2248−223.....	22 48 21.99	−22 20 27.8	0.307	18.5	r	2	16		
2250−210.....	22 50 38.10	−21 01 09.2	0.72	20.9	r	1	8		
2254−248.....	22 54 58.79	−24 53 39.9	0.54	19.8	r	2	16		
2255−228.....	22 55 18.28	−22 52 36.0	...	23.5:	r	1	20		
2256−207.....	22 56 01.79	−20 43 53.2	0.87	21.9	r	1	10		
2303−253.....	23 03 45.96	−25 23 05.7	0.73	22.3	r	1	8	N	
2304−257.....	23 04 24.47	−25 42 59.7	...	...	K	1	*	N	
				>24	r	1	3		
2307−282.....	23 07 25.95	−28 14 08.7	...	22.2	r	1	10		
2308−214.....	23 08 07.25	−21 24 32.5	0.151	18.4	r	2	16		
2311−222.....	23 11 57.20	−22 12 13.5	0.434	20.5	r	1	2		
2313−277.....	23 13 40.27	−27 46 20.2	0.614	23:	r	1	20		
2314−211A.....	23 13 55.32	−21 11 36.0	...	22.9	i	1	18	N	
2314−211B.....	23 14 02.14	−21 09 58.9	...	20.3	i	1	18		
2314−211C.....	23 14 14.31	−21 12 05.7	...	21.3	i	1	18		
2317−223.....	23 17 14.20	−22 22 32	...	...	r	2	11		No map
2317−277.....	23 17 15.46	−27 43 50	0.173	...	r	1	18		Poor map
2318−244.....	23 18 24.49	−24 27 09.4	1.12	...	r	1	2		
2320−269.....	23 20 37.05	−26 56 30.5	0.99	23.4	r	1	8		
2321−228.....	23 21 23.94	−22 51 24.1	0.114	15.3	r	2	16		
2322−275.....	23 22 08.15	−27 35 49.4	1.27	21.8	r	1	8		
2324−259.....	23 23 59.83	−25 58 18.8	0.286:	18.3	r	1	20		
2325−213.....	23 25 58.08	−21 22 22.6	0.58	20.8	r	1	2		
2326−254.....	23 26 10.10	−25 24 35.7	...	21.1	r	1	8		
2327−215.....	23 27 02.89	−21 30 18.1	0.28	19.3	r	2	11		
2329−251.....	23 29 09.37	−25 08 42.9	...	23.5	r	1	3		
2340−219.....	23 40 48.36	−21 58 13.2	0.766	20.9	r	1	10		
2341−244.....	23 41 36.18	−24 24 21.1	0.59	20.9	r	1	18		
2343−243.....	23 43 09.37	−24 19 11.3	0.6	19.9	r	2	16		
2345−284.....	23 45 09.21	−28 25 06.1	0.028	...	r	2	11		
2348−235.....	23 48 53.26	−23 33 47.3	0.952	22.7	r	1	20		
2351−222.....	23 51 35.94	−22 13 32.6	...	23.0	r	1	3		
2351−234.....	23 51 17.55	−23 28 10.9	1.03	21.8	r	1	6		
2355−214.....	23 55 01.08	−21 30 09.9	1.41	22.8	r	1	16	N	
2356−210.....	23 56 45.53	−21 04 39.5	0.096	17.04	r	2	11		
2359−259.....	23 59 44.62	−25 05 57.2	...	20					

NOTES.—(1) For sources noted as "Unidentified" we list the radio position as derived from either our VLA images or from the MRC when VLA observations are not available. Positions listed to the nearest arcsecond of declination are all radio positions. (2) All of the magnitudes listed are measured in a 4″ diameter aperture in the Thuan-Gunn *r*- band, even when the image shown in Fig. 1 is in a different pass-band. (3) The run numbers dedenoted by asterisks are IR imaging runs that will be described elsewhere. (4) Field of view (FOV) codes are as follow: 1 = 66″ × 66″(2.5 m + TI), 2 = 87″ × 87″ (1 m + TI), 3 = 71″ × 71″ (2.5 m + IR), 4 = 170″ × 170″ (Sky Survey), 5 = 59″ × 59″(2.5 m + Tek No. 1), 6 = 51″ × 51″ (2.5 m + Tek No. 2), 7 = other. 5. An "N" in the column headed "Notes" means that there is a note for this object in § 4 of the text.

[a] Right ascensions in hours, minutes, and seconds.

[b] Declinations in degrees, arcminutes, and arcseconds.

source position (i.e., centroid or midpoint). For small ($\leq 5''$) and unresolved sources we required that the candidate identification lie no more than 1.″5 from the radio position to be considered a firm identification. For larger sources we were occasionally required to choose between more than one candidate identification; the candidate closest to the midpoint was usually chosen. In most cases the identification process was straightforward, and we found it sufficient to simply compute the offset from one of the secondary reference stars to the radio position to make the identification. Once the source was identified, a precise optical position was computed from the centroid of the identification (usually a faint galaxy) and the secondary frame solution. When less than three secondary reference stars were within the CCD field, the position of the identification was computed from the offset from a single star, after correcting for the rotation of the CCD columns with respect to north-south.

In several cases, more than one object remained a plausible identification after the final astrometry, and spectroscopic observations (Paper IV) were needed to decide which one was correct. The object with the stronger lines was chosen as the identification. This procedure is not as arbitrary as it may sound because the emission-line equivalent widths of radio galaxies are typically several times those of ordinary field galaxies (e.g., McCarthy 1993).

The r magnitude of each source identification was measured in a series of apertures ranging from 0".5 to 10", and a growth curve was determined. Local sky was determined by computing the median within a 3" wide concentric annulus with an inner radius 4" to 8", the exact location of which was chosen to avoid contamination from nearby stars or galaxies. When nearby objects could not be avoided, they were edited out of the image before the photometry was performed. There are several objects that are too close to foreground stars or galaxies for this procedure to succeed, and their magnitudes are consequently highly uncertain, i.e., ± 0.5 mag, and these are noted below. The r magnitudes listed in Table 2 refer to a 4" diameter aperture. For the brightest galaxies the 4" aperture magnitude grossly underestimates the total magnitude.

4. RESULTS

Table 2 lists each radio galaxy or empty field by its IAU name based on the 1950 source position in the MRC, its 1950 position, the provisional redshift when available, the r magnitude within a 4" diameter aperture, the telescope and observing run for which the identification image was obtained, a code number for the size of the image in Figure 1, and a brief comment. The positions refer to the optical or infrared identifications as derived above, except for those sources noted as unidentified. For the latter the VLA radio positions are listed. There are 452 entries in Table 2, several more than the difference between the original catalog of 558 sources and the 110 quasar and BL Lac identifications. This occurs because a few of the sources listed in the MRC were found to be multiple in our VLA images. The identification for these sources are included here, and those which are not part of the complete radio sample are also identified as such in the notes. The redshifts listed in Table 2 are provisional only. Final precise redshifts and detailed notes concerning the spectra will be presented in Paper IV. The redshift presented here should be accurate to $\delta z \sim 0.05$.

Figure 1 (Plates 6–28) presents finding charts for nearly all of the radio galaxies. Each image is a 200 × 200 pixel subsection of a larger CCD or infrared camera image with north at the top and east to the left. The radio source identification is positioned at the central pixel in nearly all cases, but for a few objects this was either not possible or desirable. In all cases two vertical and two horizontal ticks mark the identification. For the few sources that remain unidentified, we have indicated the positions of the radio components with circles 5" in diameter. For small doubles we have marked only the midpoint position.

The size of the field displayed depends on the telescope and detector used. Column (12) in Table 2 contains a code number for the field size, which is given in the notes to the table. The vast majority of the images were taken with the 2.5 m/TI CCD combination and so have a field of 66".4 × 66".4 (code 1). Many of the brighter objects were imaged with the 1.0 m and TI CCD and have a field of 87" × 87" (code 2). The infrared images are 70" × 70" (code 3), nearly the same as the 2.5 m/TI CCD images. Several of the bright galaxies were not observed with the 1.0 m telescope, and for these we reproduce 100 × 100 pixel images from the digitized SERC J sky survey films that have been rebinned to 200 × 200 pixel images with a field size of 170" × 170" (code 4). A few images were taken with the 2.5 m plus Tektronix CCD and have a field of 59" × 59" (code 5).

Here we make a few remarks on some objects that have interesting characteristics or for which the finding chart alone may not provide enough information to make the identification clear to the reader. All of the 5 GHz and 1400 MHz data referred to below are presented in Paper II.

0007−287.—The central component of this radio source lies within 2" of a $V \sim 15$ mag star, as confirmed spectroscopically by R. Hunstead and V. Kapahi with the Anglo-Australia Telescope (AAT). No other plausible identification can be seen on our CCD images.

0022−209.—There are two sources in our map; both are identified with bright galaxies in the cluster Abell 27. Only the westernmost of the two sources is strong enough to remain in the complete sample.

0023−203.—This source is 23" south of a bright star. The identification is confirmed by our K image where the contrast against the scattered light from the star is better.

0029−232.—This is a large source, and the identification is slightly uncertain. The galaxy marked is ~2" from the symmetry axis of the source. No other potential identification is visible.

0029−243.—The identification consists of two components. The SW component is close to the midpoint of the radio source and is the correct identification.

0041−224.—The 5 GHz VLA map reveals a compact component that is well off center and slightly north of the symmetry axis of the double source. Our (poor seeing) CCD images fail to reveal an object at the location of this component or anywhere else along the source axis. Our K image, however, does reveal a very red galaxy along the source axis but not coincident with the compact radio component. We believe that this red galaxy is the correct identification and that the compact radio component is most likely to be unrelated. We present both the r and K images for this source to help the reader identify the field.

0045−255.—This source is identified with the starburst galaxy NGC 253; no chart is included.

0048−233.—This source is identified with a bright galaxy that lies only ~10" north of a bright star. The CCD image was taken through clouds.

0052−241.—The identification is quite faint and does not appear clearly in the chart shown in Figure 1. Strong Lyα emission (see Paper IV) confirms that this is the correct identification.

0102−256.—The identification of this source is uncertain. The radio source is unresolved, and its position is 2" east of the galaxy marked. The positional disagreement is larger than the ±1".5 that we used as the nominal acceptance criterion.

0112−219.—This source was not observed with the VLA, and we are unable to identify it on the basis of the MRC position. We have not included a finding chart.

0113−245.—We are unable to identify the central component of the source in our 5 GHz maps. CCD images taken with the 2.5 and 1.0 m telescopes fail to reveal any object at the location of the most plausible candidate for the central component. The structure of the 5 GHz map suggests a larger source, and this is reinforced by a 1400 MHz map (see Paper II). It is unclear if the larger component is related, as no optical counterpart appears near its midpoint. In Figure 1 we show a sky survey image with the four components marked. The field of view of this image is 340" × 340"

0115−261.—This source is identified with a moderately faint galaxy located 15".5 E and 10".5 N of a much brighter

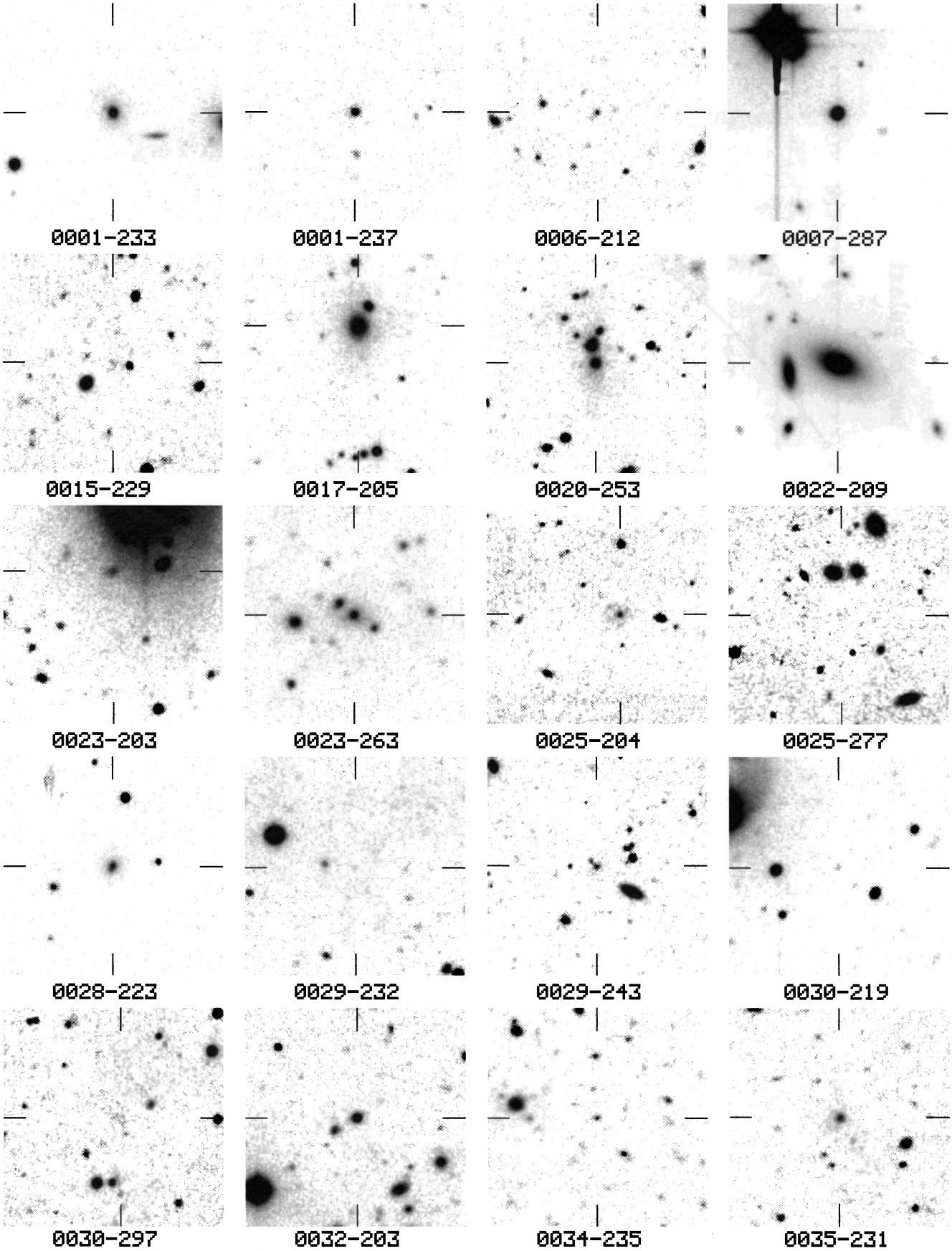

FIG. 1.—Finding charts for each of the radio galaxies in our sample. Each chart is a CCD, IR, or sky survey image with north at the top and east to the left. The IAU name for each source is marked below the chart. Those charts that were prepared from *K*-band images are marked with a "K" in the lower right corner. The position of the identification in each chart is marked by the intersection of the four tick marks at the edge of the field. The radio positions for unidentified sources are marked with a circle that is 5″ in diameter. The filter used, observing run, and field of view are listed in Table 2.

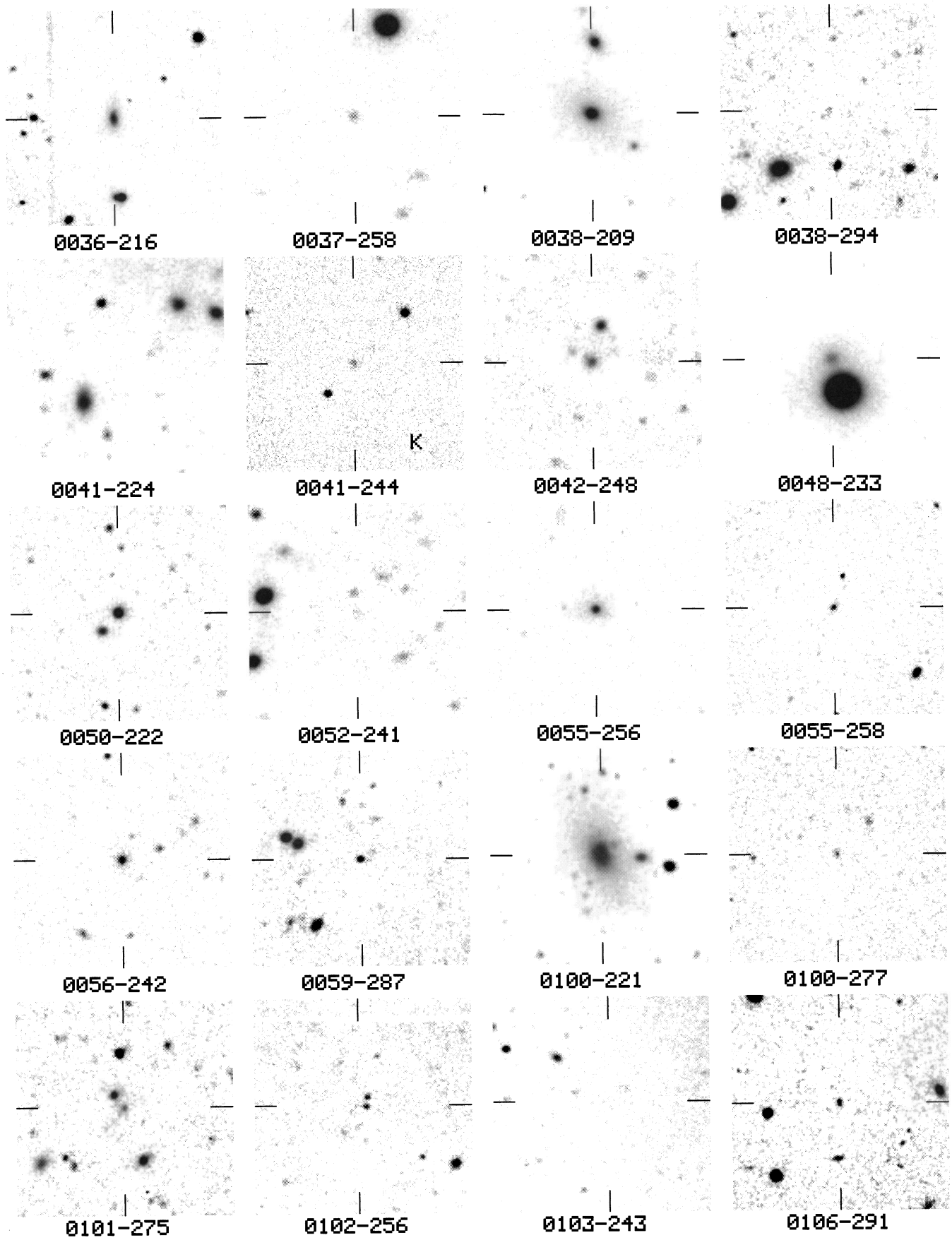

FIG. 1—*Continued*

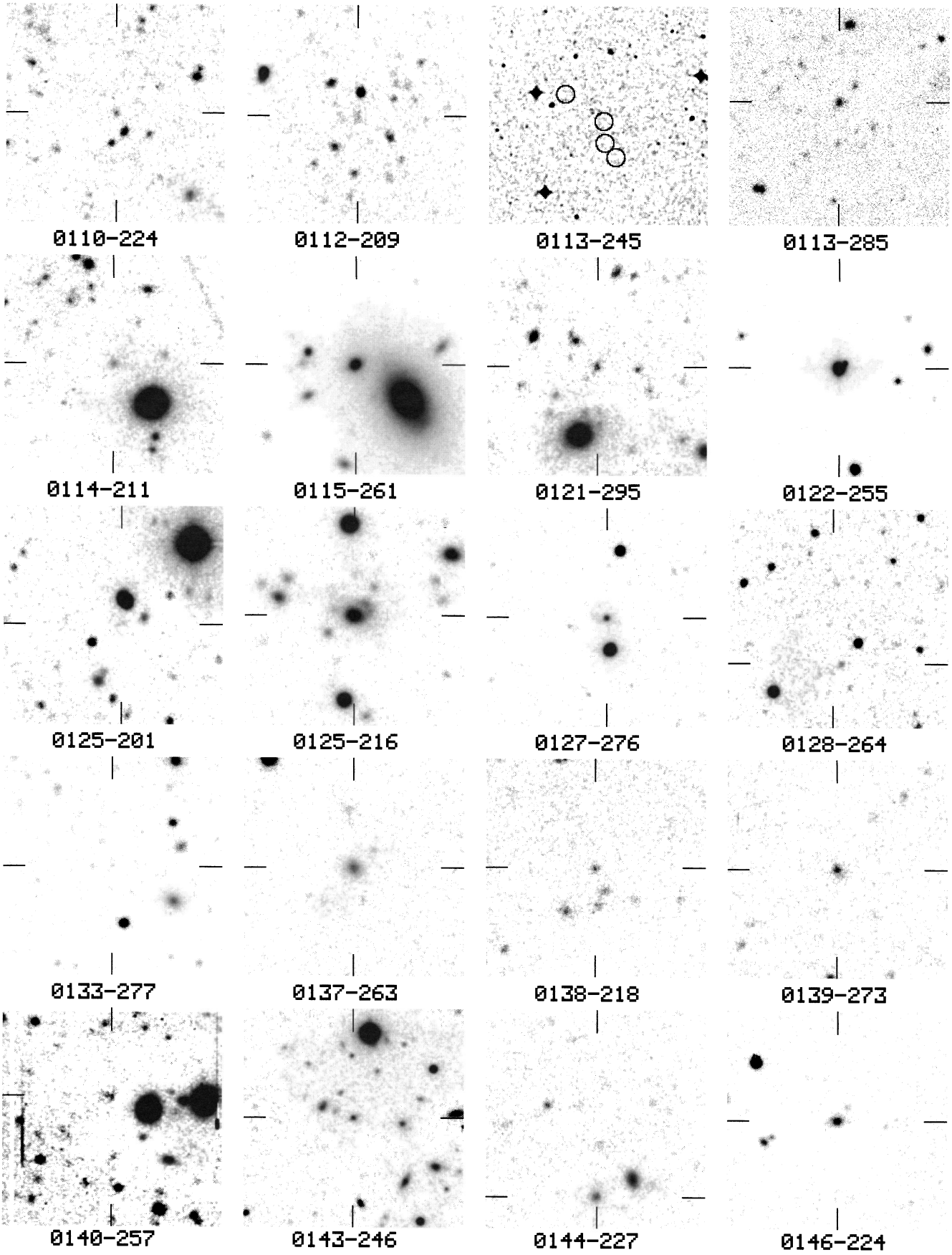

FIG. 1—*Continued*

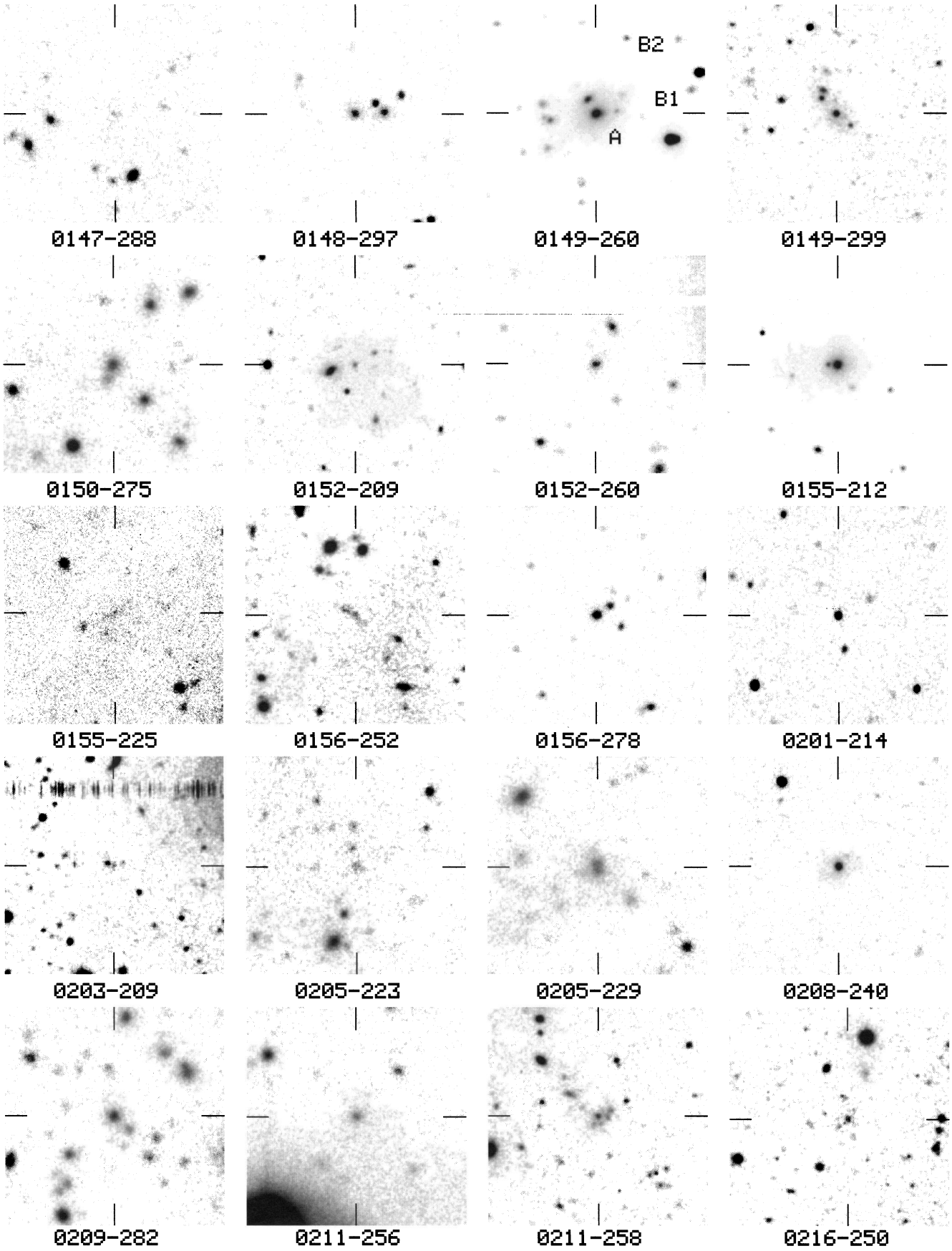

FIG. 1—*Continued*

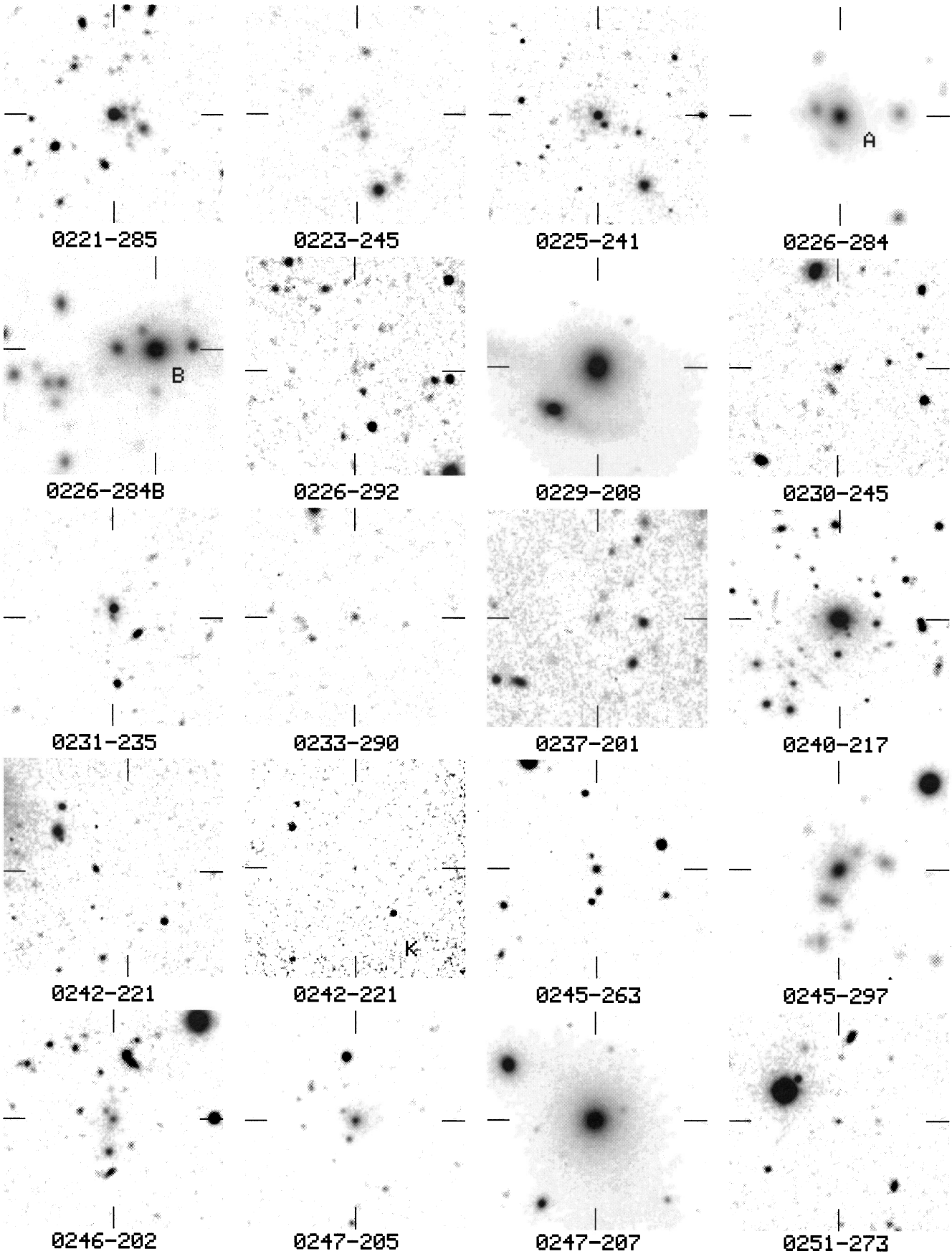

FIG. 1—*Continued*

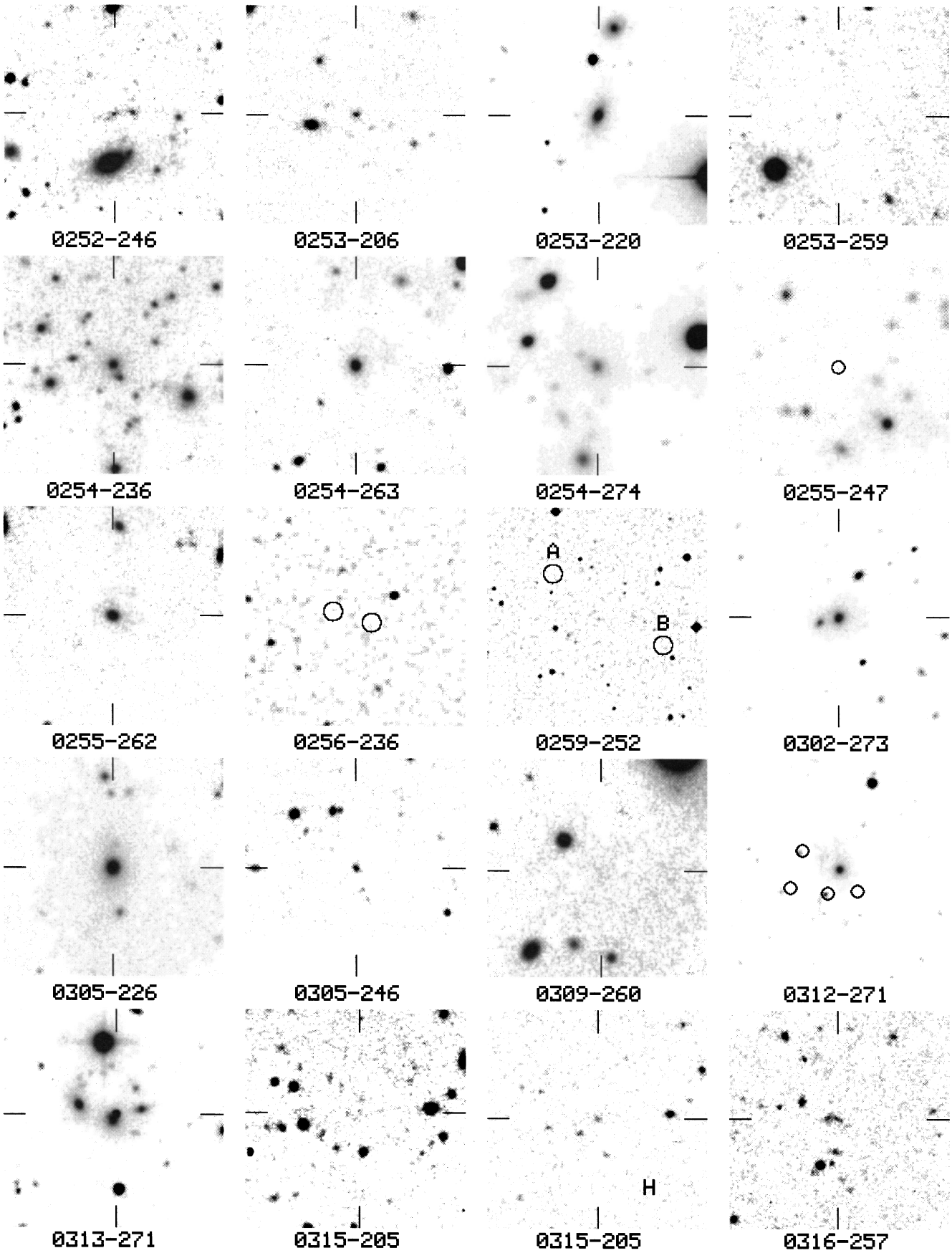

FIG. 1—*Continued*

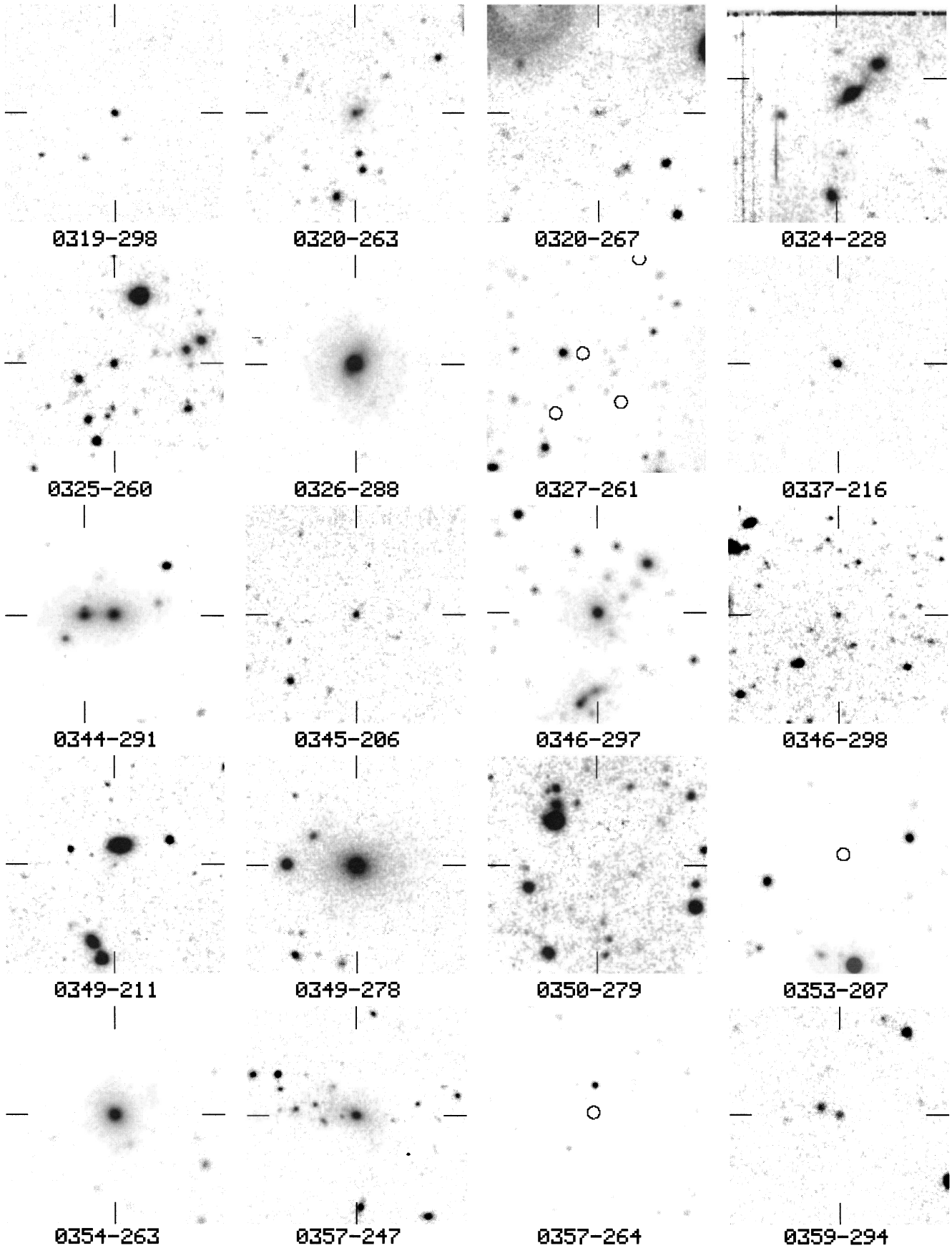

FIG. 1—*Continued*

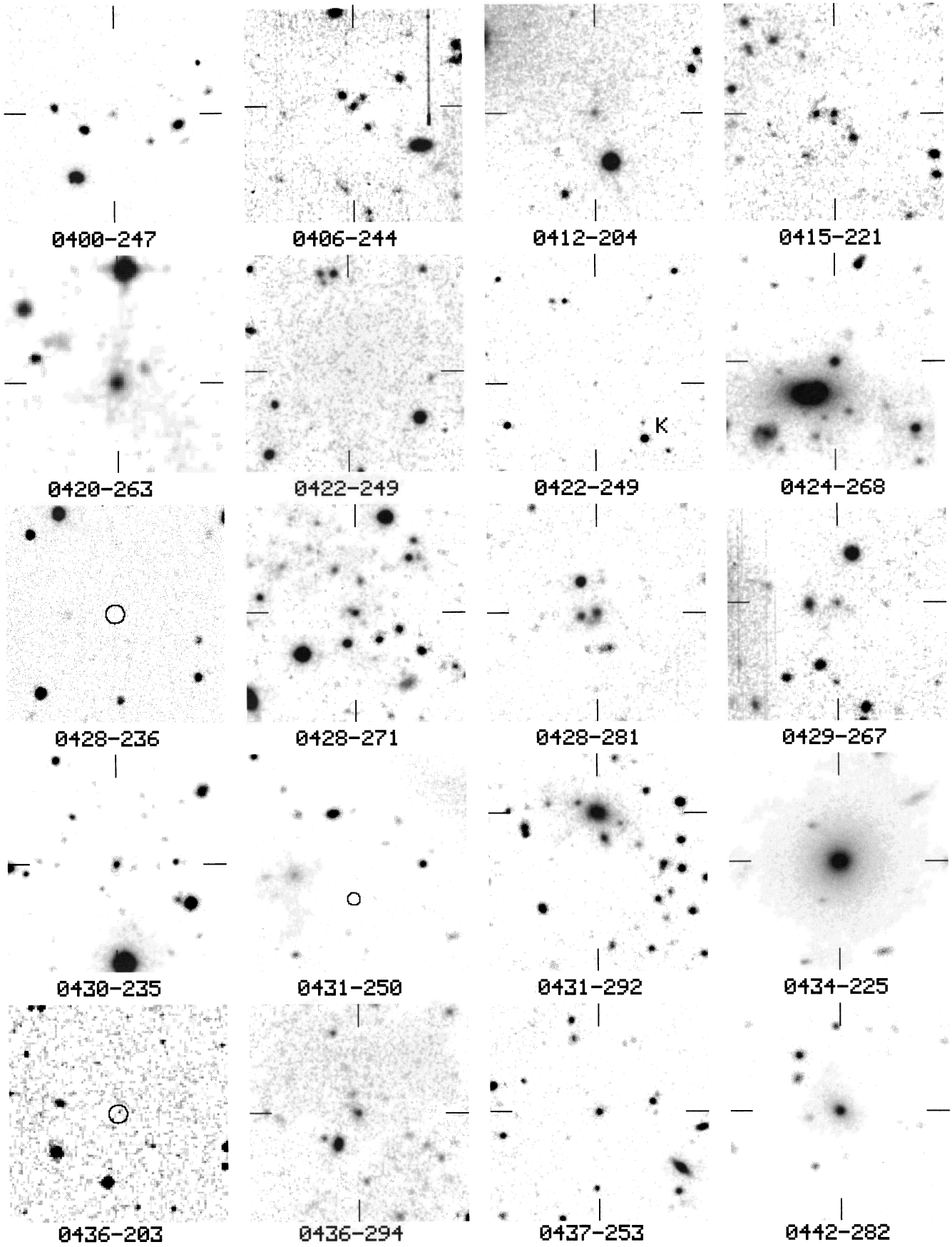

FIG. 1—*Continued*

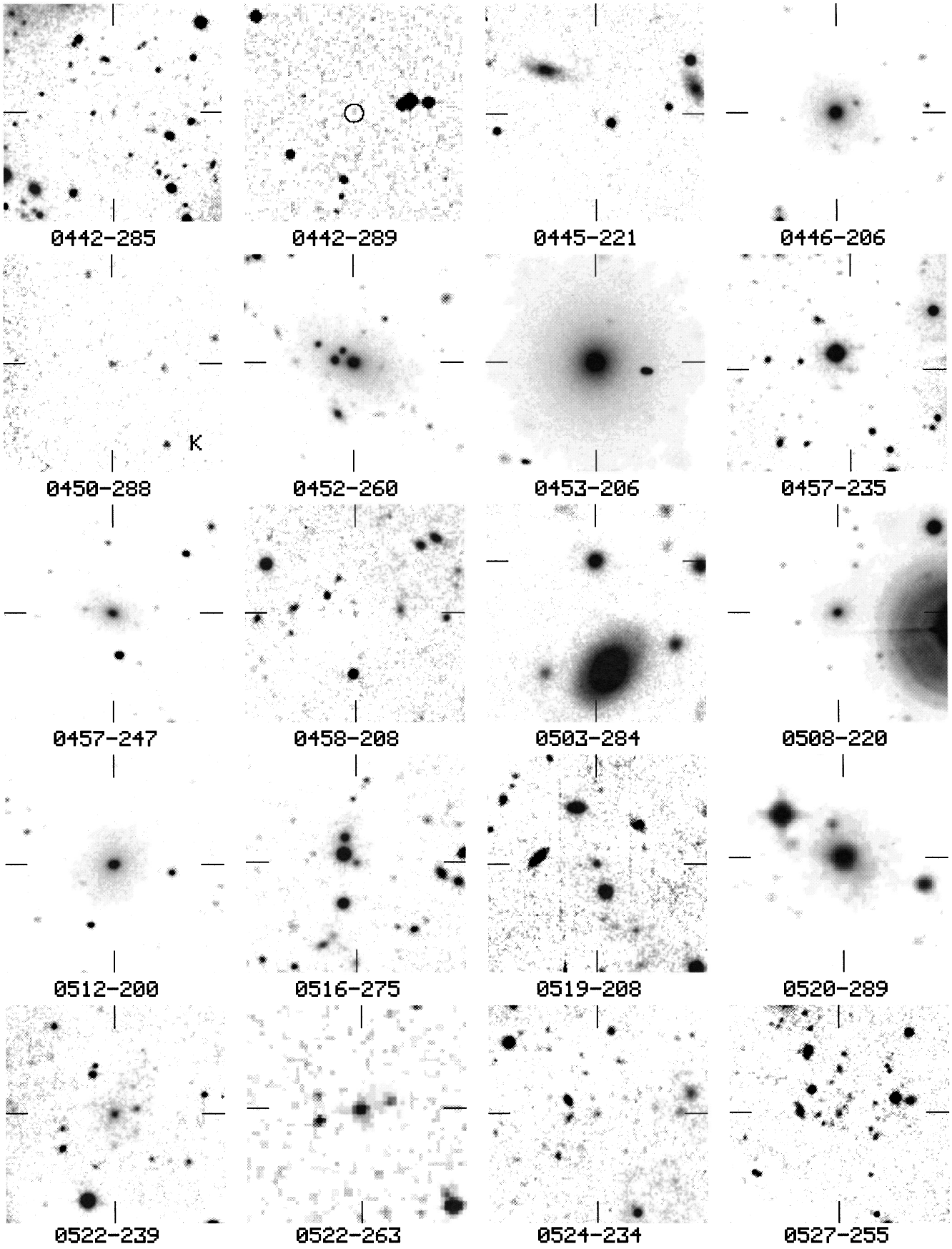

FIG. 1—*Continued*

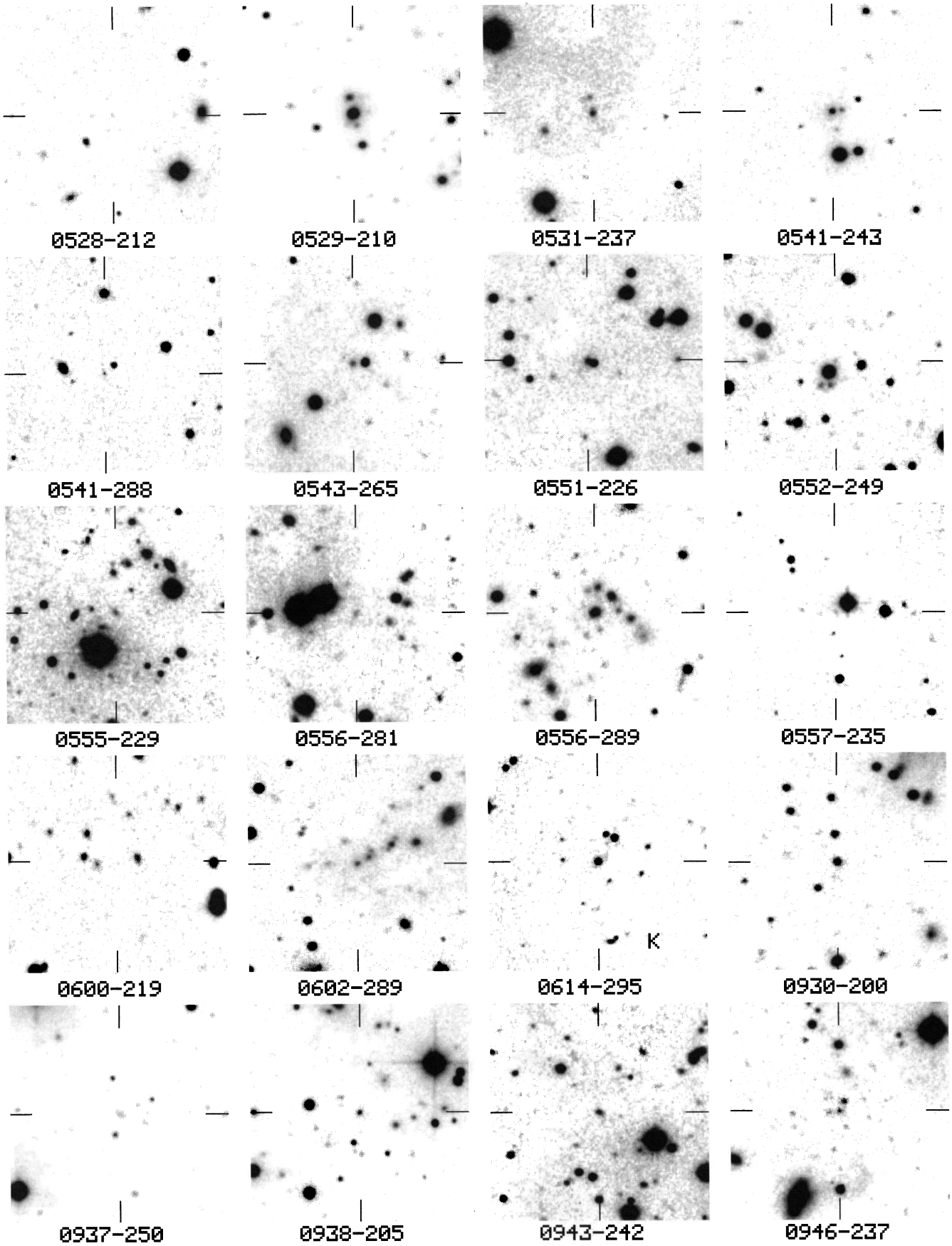

FIG. 1—*Continued*

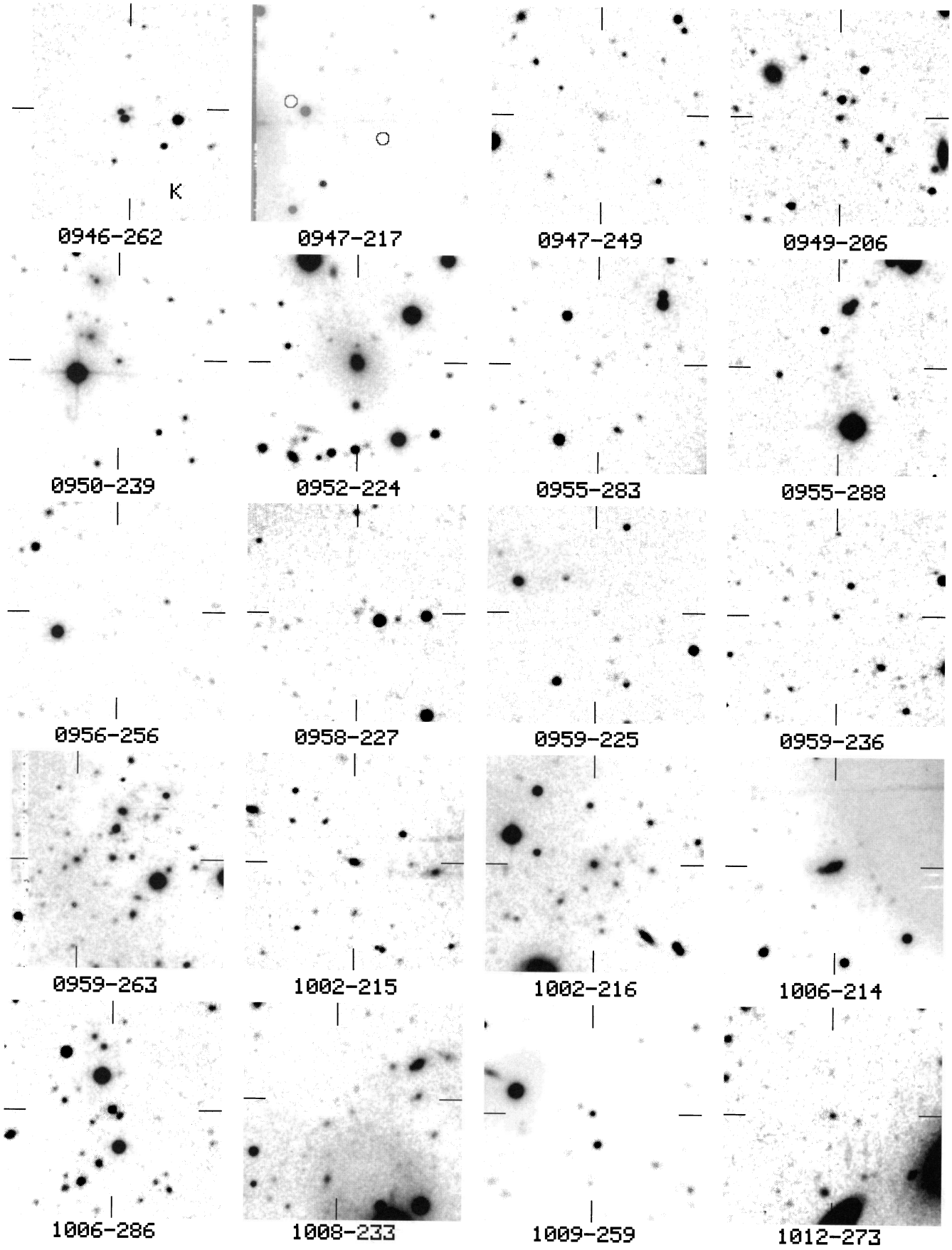

FIG. 1—*Continued*

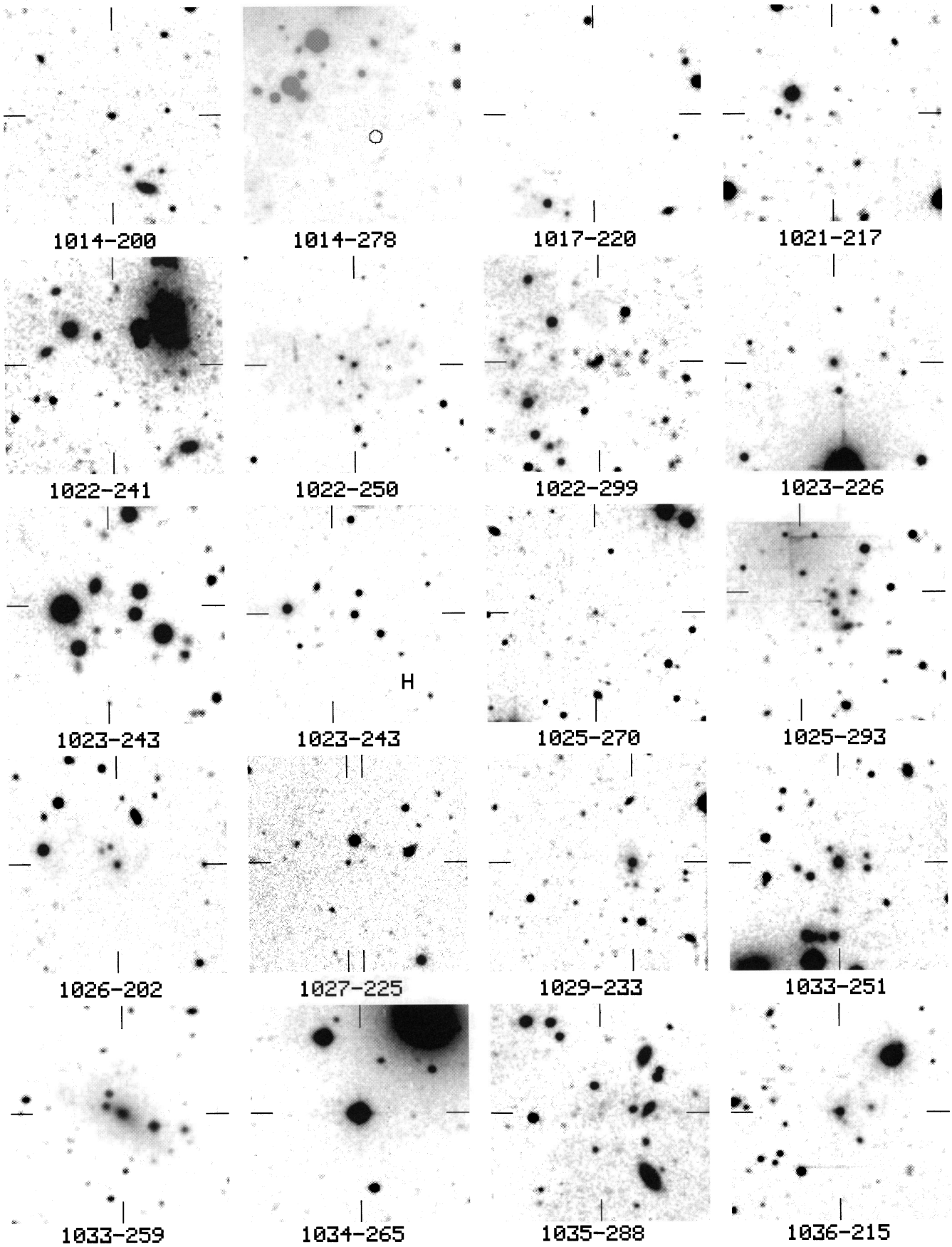

FIG. 1—*Continued*

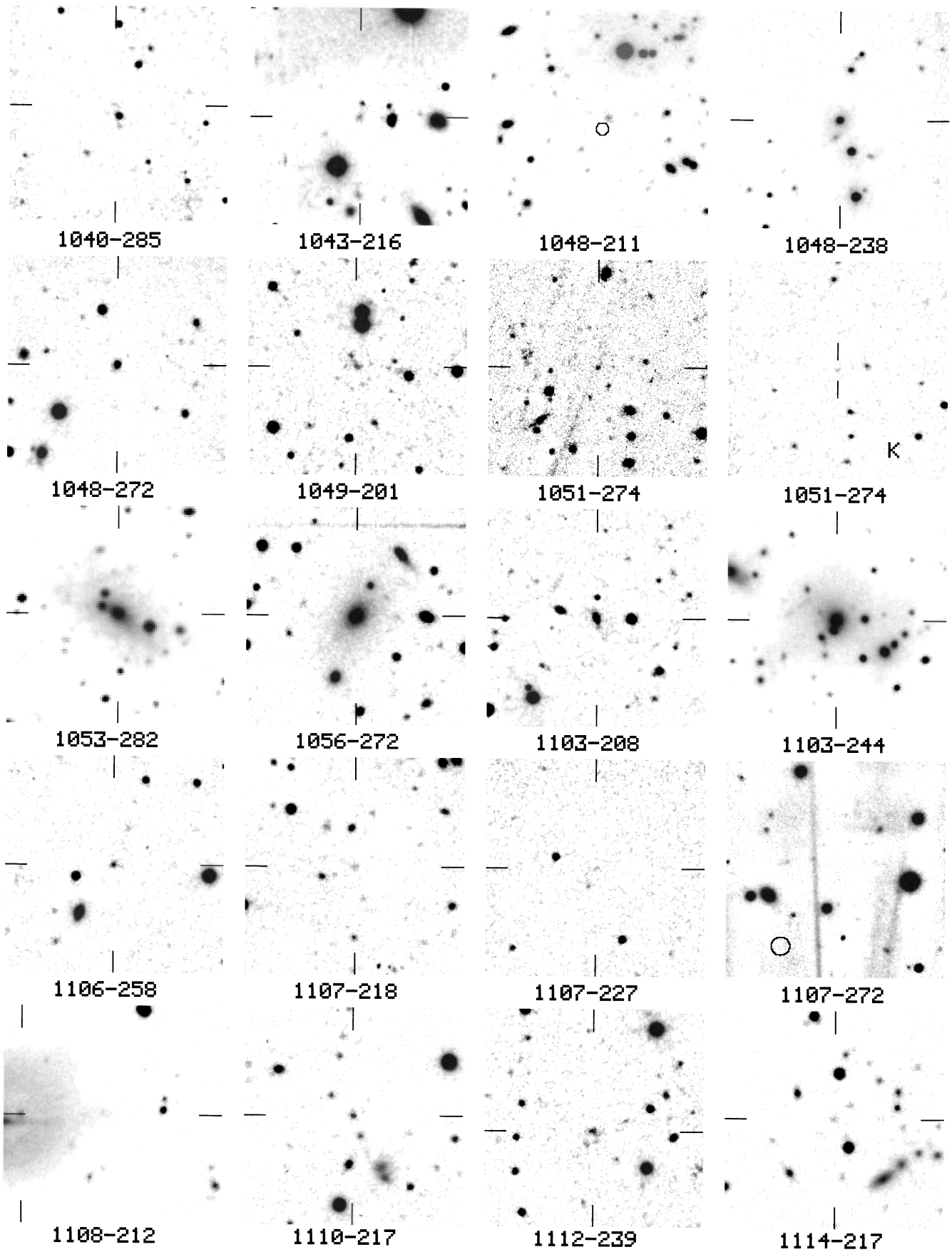

FIG. 1—*Continued*

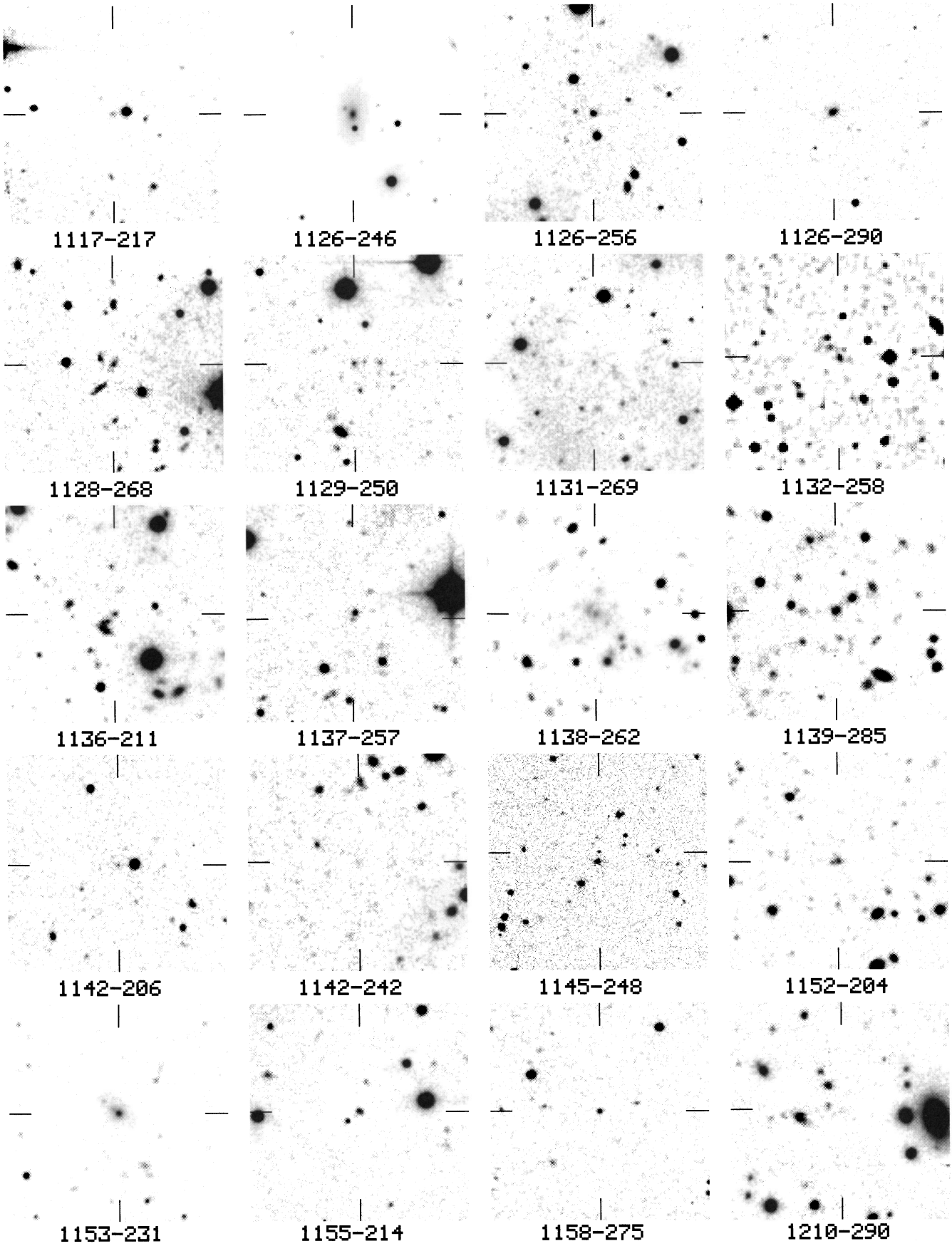

FIG. 1—*Continued*

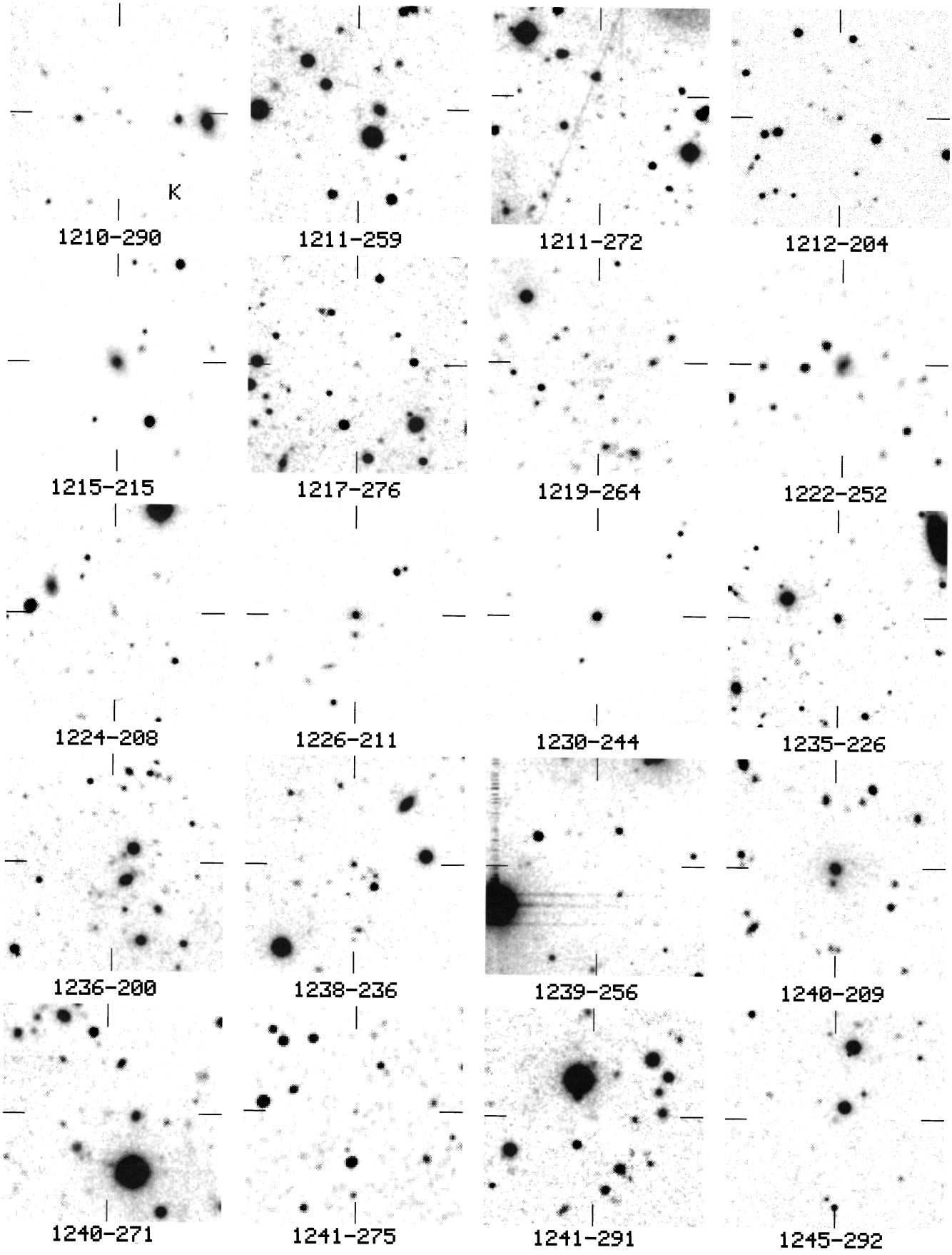

FIG. 1—*Continued*

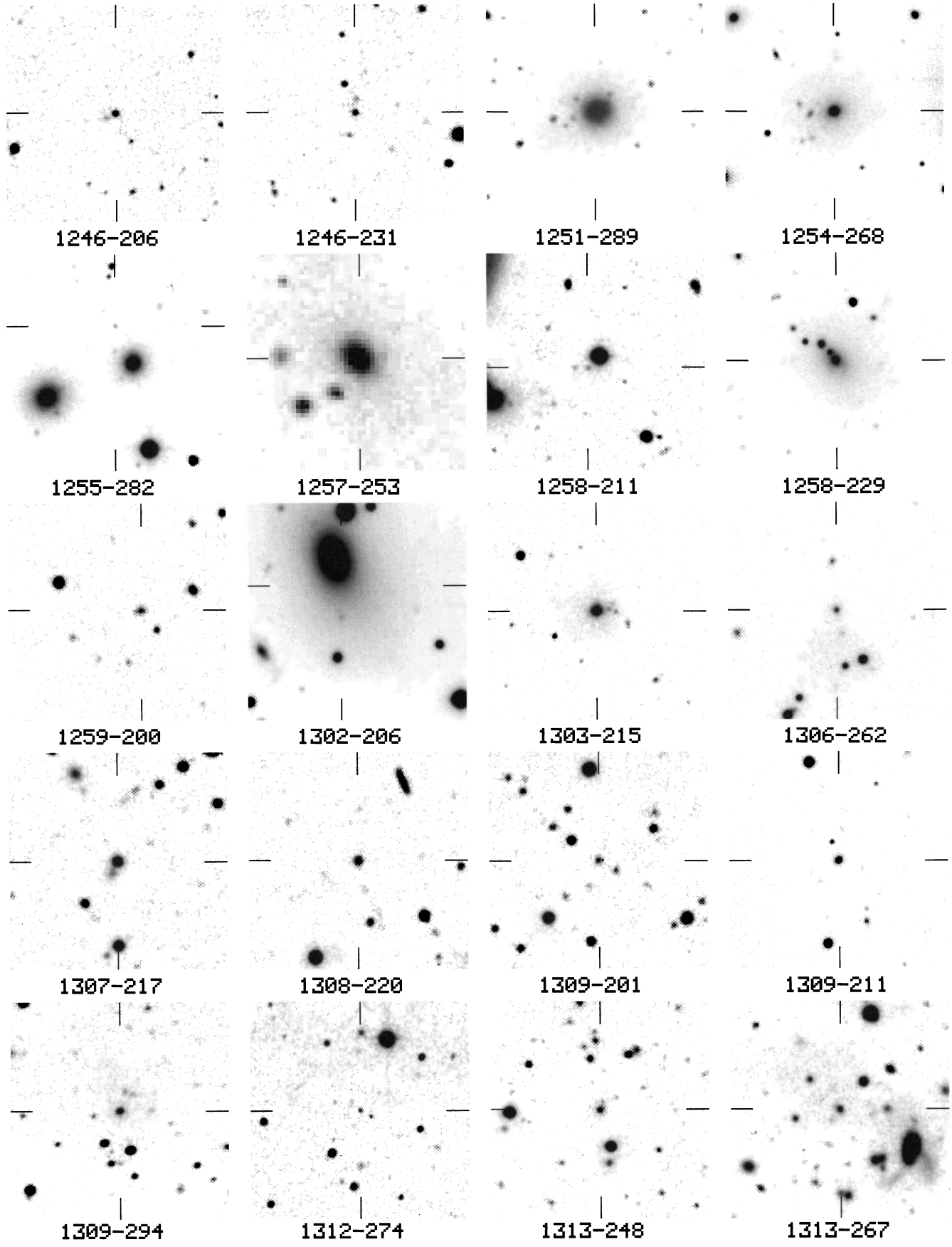

FIG. 1—*Continued*

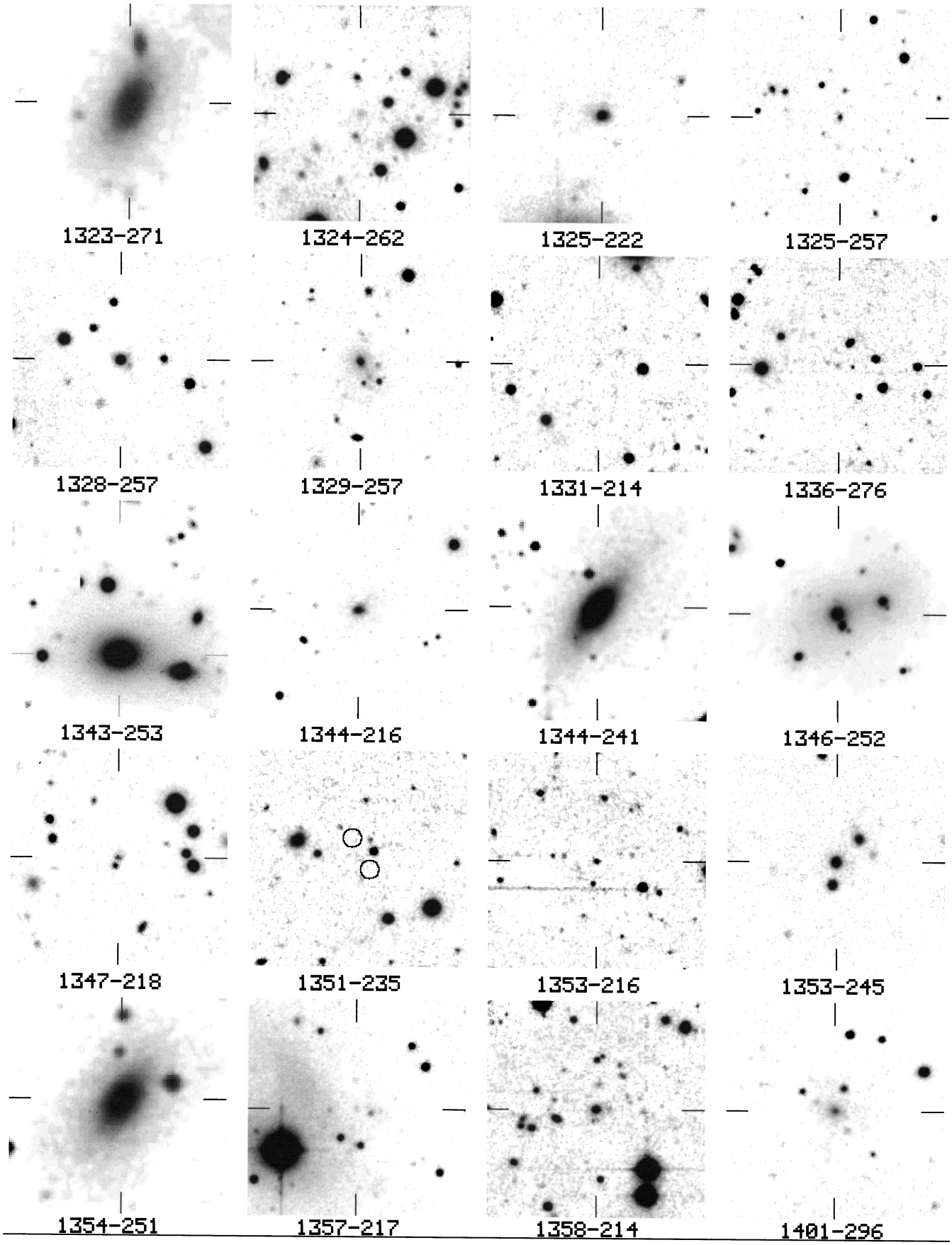

FIG. 1—*Continued*

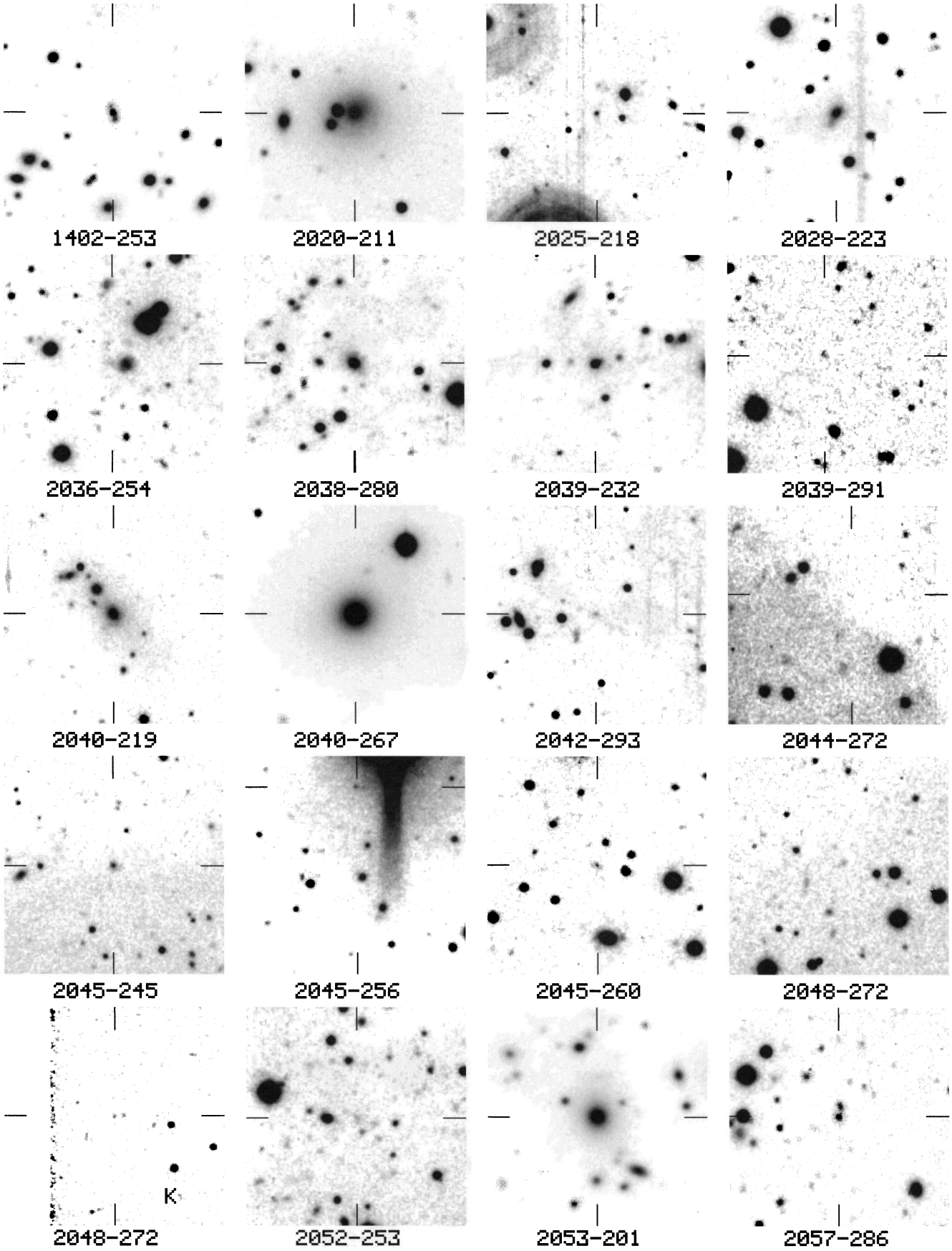

FIG. 1—*Continued*

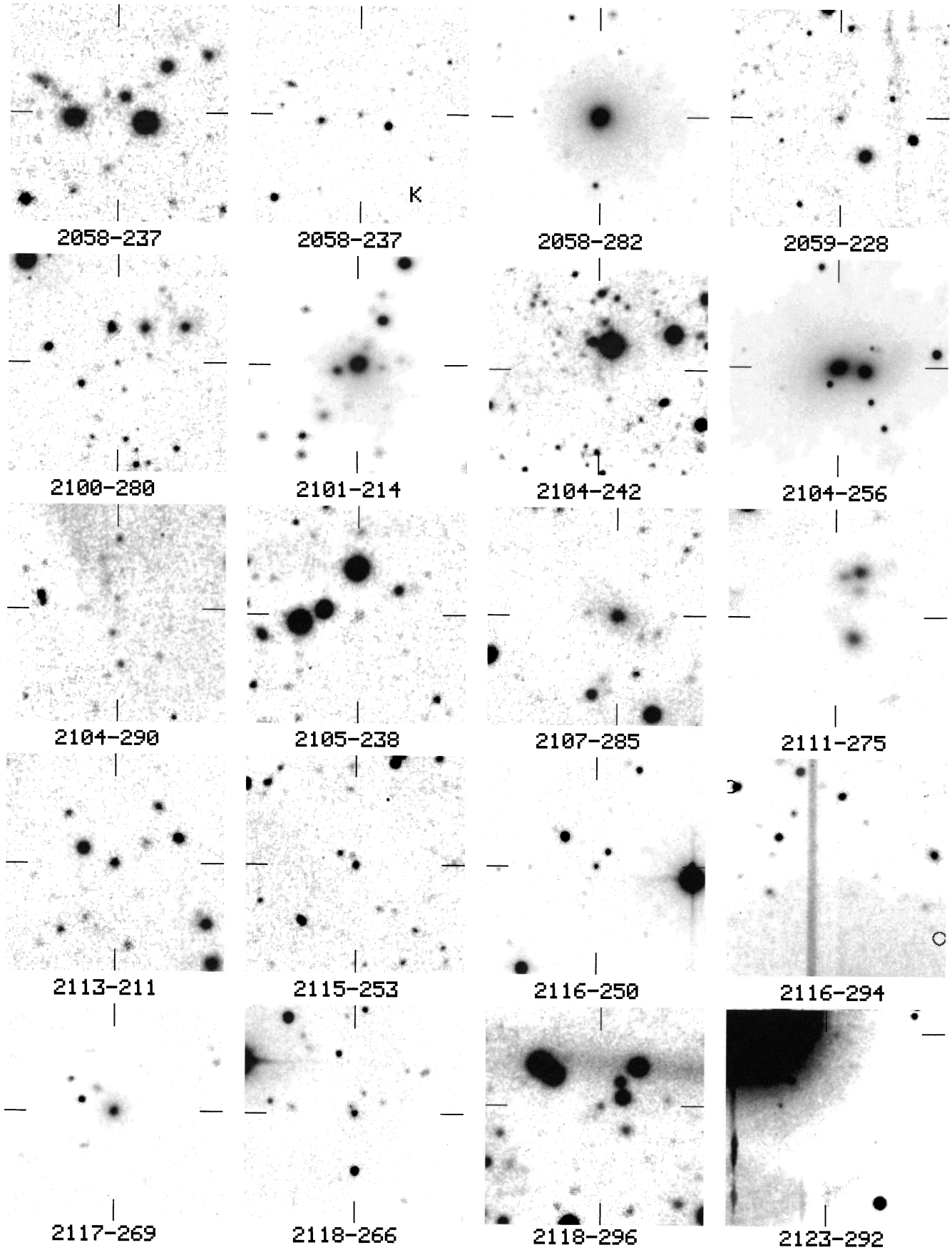

FIG. 1—*Continued*

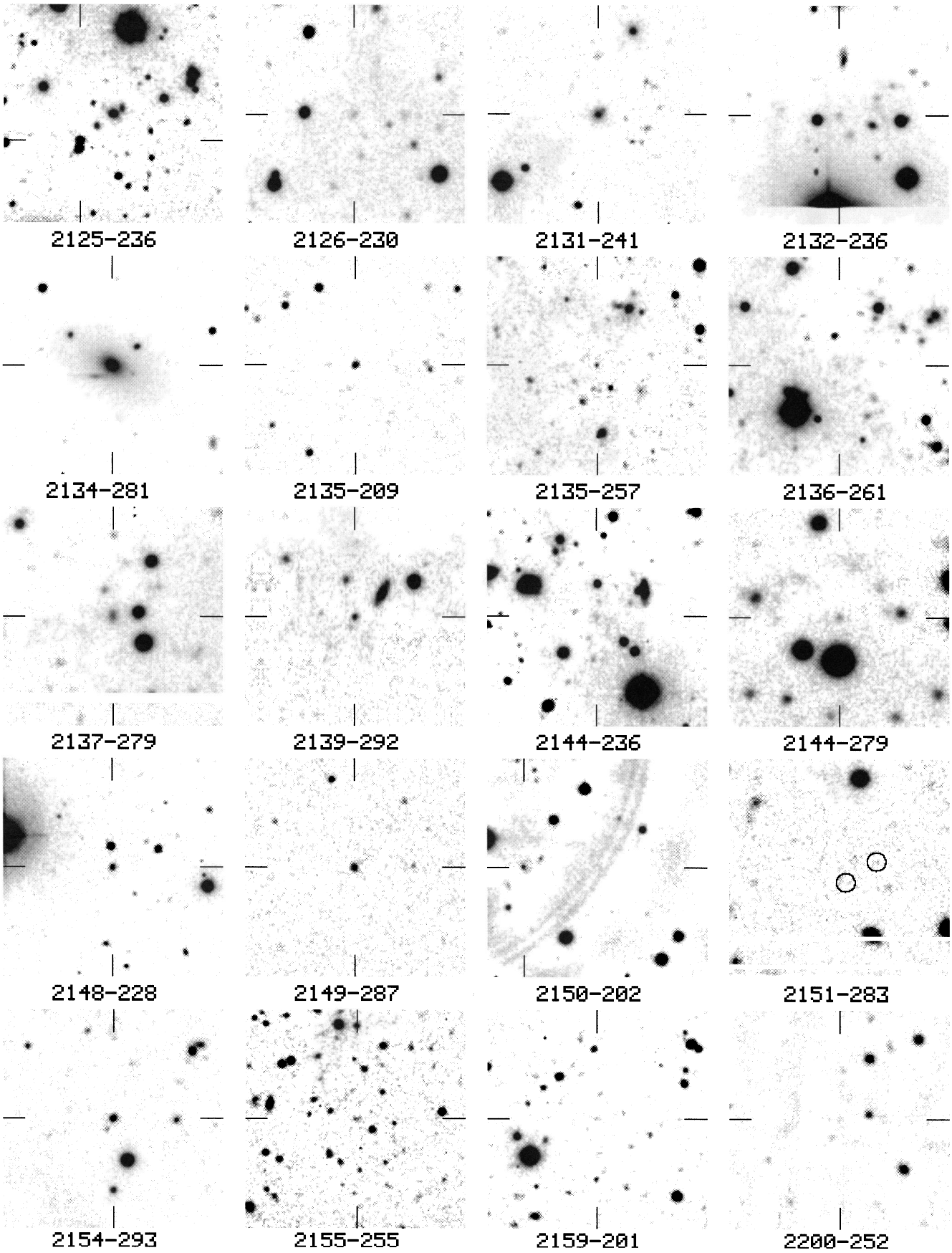

FIG. 1—*Continued*

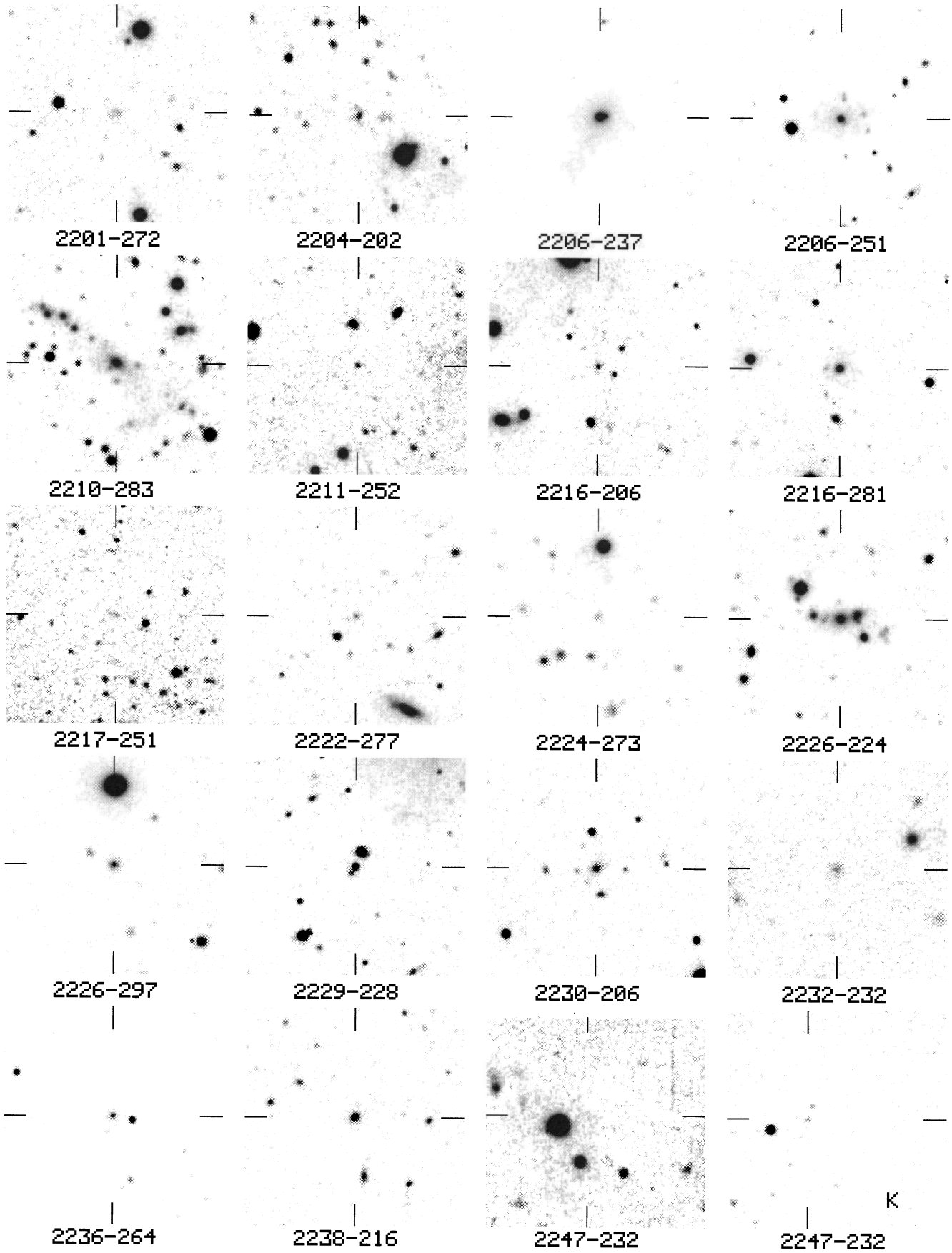

FIG. 1—*Continued*

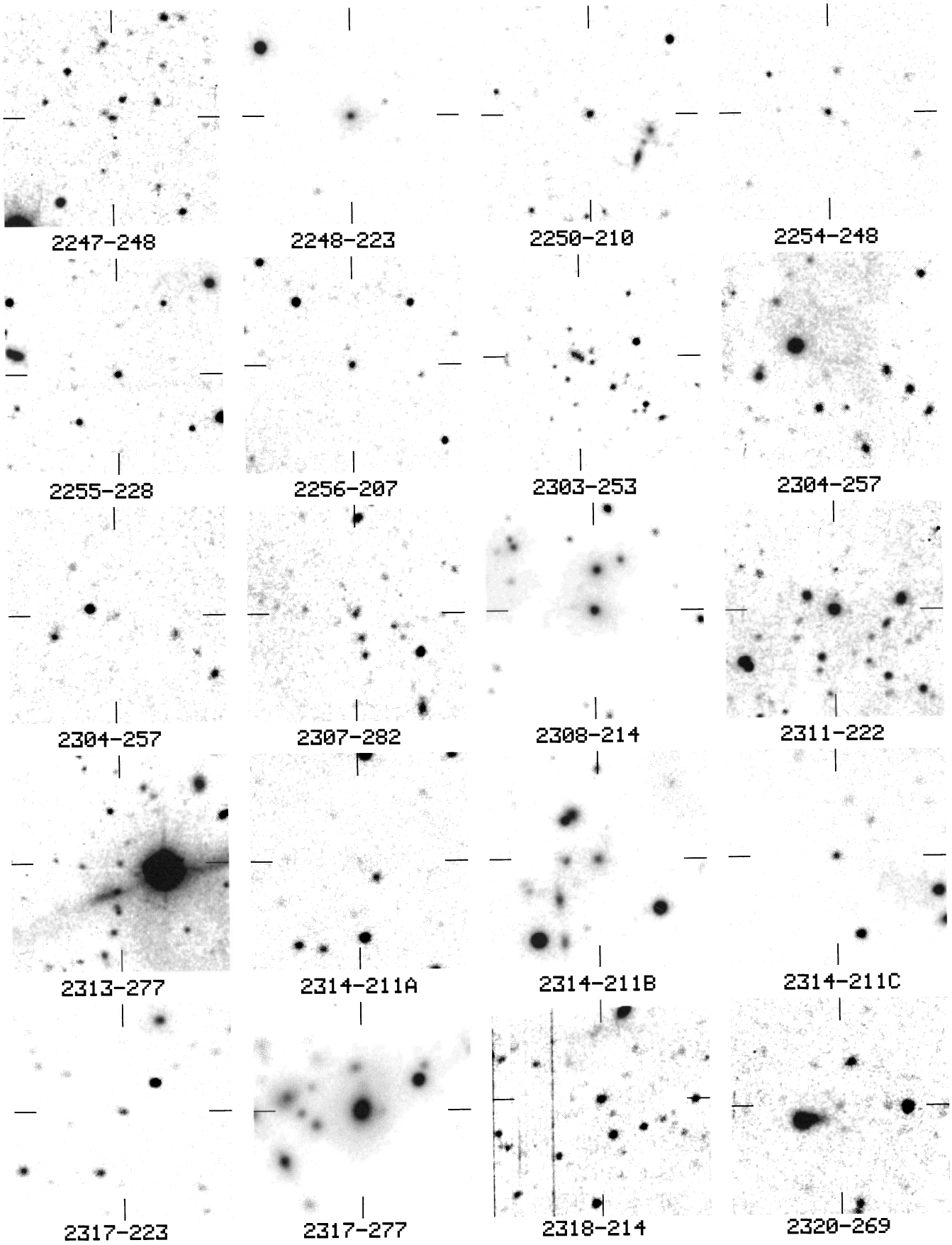

FIG. 1—*Continued*

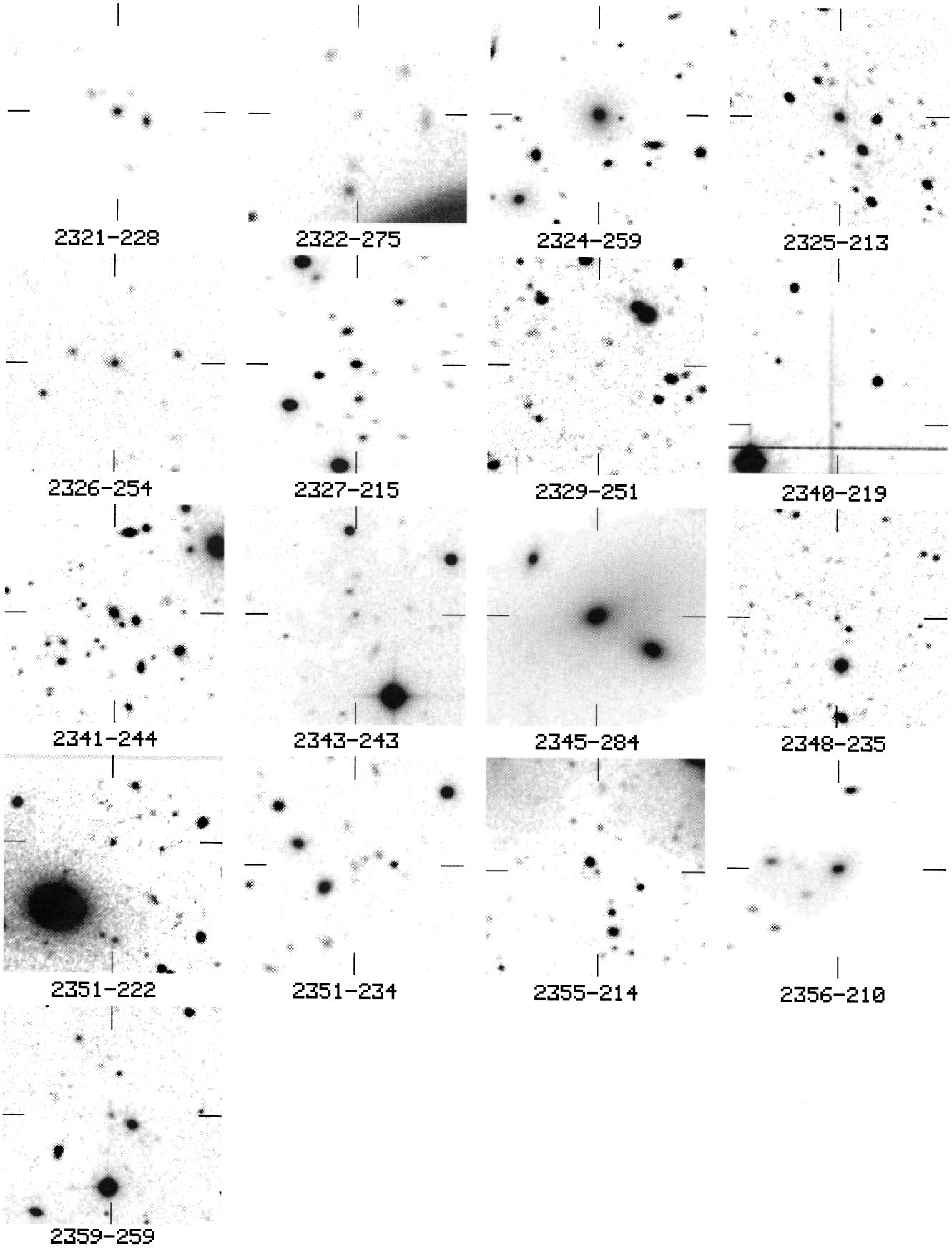

FIG. 1—*Continued*

galaxy. This source was incorrectly identified with the brighter galaxy by Ekers et al. (1989), and thus the source should not be part of their optical magnitude limited sample.

0122−255.—The central component of this triple source is coincident with the stellar object at the center of the chart in Figure 1. Spectra obtained by us with the CTIO 4 m shows this object to be a star. We detect no other potential identifications for this source.

0127−276.—Our 6 cm map reveals a single resolved component located 6″ E and 2″ S of the marked identification. Long-slit spectra obtained with the CTIO 4 m (Paper IV) reveals strong spatially extended [O III] λλ5007,4959 emission at the location of the identification and the radio source. We are confident that we have the correct identification and suspect that we are missing the western lobe of the source in our map.

0149−260.—The identification of this source is uncertain. The 5 GHz map reveals two sources, the eastern one of which is identified with the galaxy marked A in Figure 1. The other source could be identified with either of the two objects marked as B1 and B2, although we believe that B1 is the most likely identification.

0203−209.—There are three faint galaxies near the center of the field shown in Figure 1. The central galaxy is the identification for the triple source (see McCarthy et al. 1990).

0211−258.—There is a compact group of galaxies near the center of this double source. We believe that the brightest galaxy in the group is the correct identification.

0221−285.—The identification for this double source is uncertain. The presence of a star 4″ W and 4″ S of the midpoint interferes with the imaging. The faint object marked in Figure 1 lies along the radio axis but is 3″.5 from the midpoint. No other potential identifications are visible in our deep CCD images.

0226−284.—Our 5 GHz maps reveal this to be two sources, both of which are identified with bright cluster galaxies. The identifications, noted as 0226−284A and 0226−284B, are both shown in Figure 1. Source 0226−284B may fall below our 408 MHz flux density limit of 950 mJy.

0242−221.—This source is not identified on our CCD images, but our deep *K* image shows a faint galaxy within 2″ of the position of the compact radio source. The position given in Table 2 is derived from the *K* image.

0251−273.—This narrow-lined galaxy has the highest redshift in our sample ($z = 3.16$). Our *r* and narrowband Lyα images reveal no significant structure, and our *K* images also show the object to be compact.

0255−247.—The structure of this source as revealed by our 6 cm map suggests that we may be seeing only one component of a larger double source. Our CCD images reveal no potential identification at the location of the radio component seen in our map.

0256−236.—The source is a low surface brightness 46″ double, and it was resolved out in our 5 GHz observations. We do not have a CCD image of this field, and we are unable to identify the source on the digitized sky survey.

0259−252A, B.—We are unable to identify this source or even decide for certain if it is one or two sources. Our 5 GHz map is quite poor and suggests either a very large source ($\theta > 360''$) or two sources. Our 1400 MHz map reveals both components but is ambiguous as to whether it is one or two sources. We have obtained images at the positions of both components and near the midpoint with the 1.0 m telescope and fail to find any plausible candidate identifications for either the one or two source scenarios. We reproduce a 340″ × 340″ chart from the digitized sky survey with the two components marked.

0309−260.—The source is a very low surface brightness double, and the identification is also of very low surface brightness and is not easily visible in the chart shown in Figure 1.

0312−271.—The source is complex and is composed of two or more double sources. No plausible identifications for various assignments of the components to two or more sources are seen in our CCD images obtained with the 1.0 m telescope.

0315−205.—The identification for this source is diffuse and barely visible in the *r*-band, although it is easily seen at *H*. We reproduce the *r* image here but give the position based on astrometry from the *H* image.

0316−257.—This is the second highest redshift in our sample and the galaxy has a complex morphology. The western component is the correct identification for the small double source (see McCarthy et al. 1990).

0327−261.—The source is complex and is composed of two or more sources.

0349−278.—This is a well-known identification and optical spectra reveal strong emission lines extended over many arcseconds (e.g., Danziger et al. 1984).

0353−207.—We are unable to identify this unresolved steep spectrum source on our CCD images obtained with the 2.5 m telescope. We do not have a *K*-band image.

0357−264.—We have not succeeded in identifying this source. The only image that we have of this field is a 600 s exposure with the 1.0 m telescope. Deeper imaging is required.

0422−249.—The identification for this source is faint and diffuse in the optical and we do not convincingly detect it in our *r* image. The identification is well detected at *K*, and we reproduce both our *r* and *K* images in Figure 1.

0428−236.—This source is not identified on our CCD images obtained with the 1.0 m telescope.

0428−281.—The correct identification is the northwesternmost object of the three at the center of the field.

0431−250.—We are unable to identify this triple source on our *r*-band CCD images obtained with the 2.5 m telescope.

0436−203.—We have no CCD images of this source. For completeness we include the sky survey chart with the VLA position marked.

0442−289.—We have no CCD images of this source, but for completeness we include the sky survey chart with the VLA position marked.

0457−235.—The identification is 4″ W and 5″ S of the bright star near the field center. The identification consists of two components, one of which is coincident with the central component of the radio source, the other with the NE radio lobe. The NE component is seen more clearly in the *g* image than in the *r* image shown in Figure 1.

0541−288.—There are two possible identifications for this source, the object marked and the object located 4″ W and 3″ N of the center. Our *K* images show the SE object to be redder and is thus more likely the correct identification.

0543−265.—The correct identification is the easternmost object of the pair at field center.

0551−226.—The correct identification is 1.″5 E and 0.″5 N of a star and is seen more clearly at *K*.

0552−249.—The correct identification is 1.″9 W and 3.″3 N of the star near the field center.

0557−235.—The midpoint of this double source is only 4″ from a bright star. We are able to identify it only at *K* due to the scattered light from the star at *r*.

0614−295.—We do not have an *r* image of this source but have identified it on the basis of a *K*-band image, shown in Figure 1.

0946−237.—Our 5 GHz map reveals two sources, only one of which is strong enough to remain in the sample. It is identified with the southernmost of the two objects at the center of the field.

0946−262.—The identification for this double source is 1.″5 W and 2.″ N of the southernmost of the pair of stars near the center of the *K* image shown in Figure 1.

0947−217.—We are unable to identify this source. Our 5 GHz map is quite poor and reveals three components, one of which may or may not be part of the source. Our 1400 MHz map shows the source to be a double. The positions of these two components are shown on the chart in Figure 1. Neither our *r*- nor our *K*-band images show plausible candidates for the identification.

0947−249.—Our 5 GHz map reveals two sources, one of which is strong enough to remain in the sample; it is identified with a faint galaxy. The counterpart of the other source is not detected in our CCD image.

0955−283.—The correct identification is the northwest component of the double object at the center of the field.

0958−227.—There are two possible identifications for this compact source. The southeastern of the two objects near the field center is the more likely one (and is marked) but the northwestern one cannot be ruled out.

1006−286.—The northeastern of the two objects at the field center is the correct identification for this small double source.

1014−278.—We are unable to identify this unresolved source in either our deep *r*- or *K*-band images, setting upper limits of $r > 24$ and $K > 19$.

1021−217.—There is a $z = 2.4$ field galaxy 14″ east of the radio source, marked on the chart with an F.

1023−226.—Our 5 GHz map reveals both a double and a compact source. The double source is identified with the galaxy at the field center. The compact source is too weak for inclusion in our sample and lies close to a bright star.

1023−243.—This small double source is not identified in our deep *r* and *i* images obtained with the 2.5 m telescope. The identification is, however, clearly seen in our *J*, *H*, and *K* images. We show the *H*-band image in Figure 1.

1027−225.—There are two plausible identifications for this 16″ double source. Both of the potential identifications are marked with ticks in Figure 1.

1034−265.—This source lies 2.″4 E and 0.″7 S of the apparently stellar object shown at the center of the chart in Figure 1. Spectroscopy of this object by Hunstead & Kapahi with the AAT confirms that it is a star. We are unable to identify the source.

1040−285.—The identification is northeast of the star near the center of the field. We present our *J* image in Figure 1 since the contrast against the nearby star is best in this image.

1048−211.—We are unable to identify this unresolved source in either our deep *r*- or *K*-band images, setting upper limits of $r > 24$ and $K > 19$.

1051−274.—There are two possible identifications along the source axis. The *r* image shows a faint object along the radio axis, while the *K* image reveals a very red object also along the axis, but further from the midpoint. We show both images in Figure 1 and give the positions for both the *r*- and *K*-based candidate identifications in Table 2. The candidate *K*-band identification is marked with a pair of small tick marks in the center of the chart.

1107−272.—We are unable to identify this source in large part because of the presence of strong scattered light from a bright star south of the radio position.

1108−212.—The identification for this triple source appears to be a galaxy ∼15″ from a bright star.

1117−217.—This double source is identified with a galaxy in our *K*-band images. It is not seen in our (low quality) *r*-band image. Our *K* image is shown in the chart in Figure 1.

1132−258.—This source was identified with a stellar object. Spectroscopy with the AAT showed this object to be a star. The positional coincidence between the radio position and the star is such that we have not attempted to image this source to seek a fainter identification.

1136−211.—The correct identification is the northwesternmost of the three objects at the center of the field.

1137−257.—The identification for this source is uncertain. The object marked in Figure 1 lies 4″ east of the compact radio source.

1138−262.—The identification for this bent triple source is highly complex. The image shown is the sum of several *r* images for a total of more than 6000 s of integration.

1145−248.—There are two possible identifications for this small triple source. The northern object is closer to the midpoint (and possible core) of the source, while the southern object is brighter. We suspect that the northern component is the correct identification, and it is marked on the chart in Figure 1.

1210−290.—Our deep *r* and *i* images fail to reveal an identification for this 5″ double source. Our *K*-band images, however, clearly reveal the identification and a very red companion object. We show both our *r* and *K* images to help the reader recognize the field.

1219−264.—The identification of this large triple source is a very diffuse and low surface brightness galaxy.

1239−256.—The identification for this source is faint and diffuse. Figure 1 shows an *I*-band image; the identification has $I = 23$.

1245−292.—The identification for this source lies 2.″5 E and 4″ S of the star near the field center.

1255−282.—The identification for this source appears stellar on our images obtained with the 1.0 m telescope. The source is a 45″ double with bright bridge emission. This source may be a quasar.

1258−211.—The potential identifications for this small double consist of two components aligned east to west and just to the southeast of the star near field center. Our astrometry places the radio midpoint closer to the westernmost object, and its redder color also suggests that it is the correct identification. It is possible, however, that the two optical components are extranuclear light associated with the alignment effect and that the nucleus lies between them.

1302−206.—This small double source is obscured by a bright foreground galaxy.

1307−217.—There are two plausible identifications for

this source. The northern source is brighter and closer to the radio midpoint and possible central component and is more likely to be the correct identification.

1334−296.—This source is identified with NGC 5236; no chart is included.

1343−253.—The identification is the bright elliptical south of the field center.

1351−235.—We have not been able to convincingly detect an identification for this double source, despite repeated efforts in both the visible and near-infrared. The identification appears to be fainter than $r > 24$, $K > 19$.

2028−223.—This source was not observed with the VLA, and we are not able to identify it on the basis of the MRC (Large et al. 1981) position.

2036−254.—The correct identification is a faint galaxy 4″ east of a brighter foreground galaxy seen near the center of the chart in Figure 1.

2039−291.–The identification for this double source is uncertain. There is a faint galaxy detected at both *r* and *K* lying 4″ north and west of the midpoint, nominally too far to be considered a secure identification. There is some low surface brightness radio emission near the faint galaxy so we consider it as a possible, but unlikely, identification.

2044−272.—There is a very faint galaxy at the position of this unresolved source, and we consider it a tentative identification.

2045−256.—This source is identified with a faint galaxy that lies just south of a bright star. It is too close to the star to allow spectroscopy.

2048−272.—The identification for this small double source is not visible in either our deep *r*- or *I*-band images. It is clearly seen in our deep *K* image, and optical spectroscopy has confirmed it to be the correct identification.

2057−286.—The correct identification is the southernmost of the two objects near the field center.

2058−237.—The identification is only marginally detected in our *r*-band CCD images, but it is well detected at *K*.

2104−290.—This large double source is identified only in our deep *K* images.

2111−275.—Our *r* image was taken in very poor seeing and the identification is only marginally visible. We have included a *K* image which shows the identification more clearly.

2116−294.—We have not been able to identify this large double source. There are no galaxies brighter than $r \sim 22$ within 10″ of the midpoint.

2123−292.—The identification of this double source lies only 35″ from a very bright star and is not easily seen in the chart in Figure 1.

2131−241.—The identification is a galaxy 1″ northwest of a star visible at the center of the chart in Figure 1.

2247−232.—The identification for this source is quite faint and is not easily seen in the reproduction of our *r* image in Figure 1. For clarity we have also included a *K*-band image. The radio galaxy is southeastern of the two galaxies appearing at the meeting of the tick marks in the *K* image.

2303−253.—The identification of this source consists of a chain of galaxies, the southwesternmost lying closest to the radio core. A 6 cm map and larger optical image of this source is given in McCarthy et al. (1991).

2304−257.—We are able to identify this galaxy only at *K*, even though our *r* images are fairly deep. Both the *r* and *K* images are shown in Figure 1 to aid in the recognition of the field.

2314−211.—Our 6 cm VLA map shows this to be three sources, which we designate A, B, and C. We show separate finding charts with the identifications marked for each source. Sources 2314−211 A and B do not belong in the complete sample as their 1410 MHz flux densities imply that they fall below our 408 MHz flux density limit.

2355−214.—The identification for this small double source is the southwesternmost of the two objects at the center of the field.

5. SUMMARY

We have presented optical/near-IR identifications and finding charts for a large and complete sample of low-frequency selected radio galaxies. This sample is well suited to a wide range of statistical studies as well as to detailed investigation of selected subsamples. In subsequent papers in this series we will provide all of the remaining basic data that is needed to fully utilize the survey data.

We gratefully acknowledge the assistance of the support staffs of the Las Campanas and Cerro Tololo Observatories as well as that of the National Radio Astronomy Observatory. In particular, we thank M. Hernandez, P. Ugarte, and H. Terrado at CTIO, and F. Perralta, H. Olivares, and O. Duhalde at LCO. We also thank I. Thompson, D. Murphy, and A. Sivaramakrishnan for their work in the development of the CCD and near-IR cameras used in this program. P. M. was supported by a Hubble Fellowship during part of the time that this investigation took place. The research of W. v. B. was performed at IGPP/LLNL under the auspices of the US Department of Energy under contract W-7405-ENG-48. P. M. C. and V. K. gratefully acknowledge the support of the American Astronomical Society through a Chretien grant. We thank Liz Doubleday for her expert assistance in the preparation of the manuscript.

REFERENCES

Allington-Smith, J. 1982, MNRAS, 199, 611
Allington-Smith, J., Lilly, S. J., & Longair, M. S. 1985, MNRAS, 213, 243
Baum, S. A., & Heckman, T. 1989, ApJ, 336, 702
Bennet, A. S. 1962, MmRAS, 68, 163
Chambers, K., Miley, G., & van Breugel, W. 1990, ApJ, 363, 21
Condon, J. 1984, AJ, 287, 461
Danziger, I. J., Fosbury, R. A. E., Goss, M. W., Bland, J., & Boksenberg, A. 1984, MNRAS, 208, 589
Djorgovski, S., Spinrad, H., McCarthy P., Dickinson, M., van Breugel, W., & Strom, R. 1988, AJ, 96, 836
Downes, A. J. B., Peacock, J. A., Savage, A., & Carrie, D. R. 1986, MNRAS, 218, 31
Dunlop, J., Peacock, J. A., Savage, A., Lilly, S. J., Heasley, J. N., & Simon, A. J. B. 1989, MNRAS, 238, 1171
Eales, S. A. 1985a, MNRAS, 217, 149
———. 1985b, MNRAS, 217, 167
———. 1985c, MNRAS, 217, 179
Ekers, R. D., et al. 1989, MNRAS 236, 737
Fanti, C., Fanti, R., Ficarra, A., & Padrielli, L. 1974, A&AS, 18, 147
Hill, G. J., & Lilly, S. J. 1991, ApJ, 367, 1
Jenkins, C. J., Pooley, G. G., & Riley, J. M. 1977, MmRAS, 84, 61
Kapahi, V. K., Hunstead, R., Baker, J., Subrahmanya, C. S., & McCarthy, P. J. 1996a, ApJ, submitted (Paper III)
Kaphahi, V. K., van Bruegel, W. J. M., Athreya, R., McCarthy, P., & Subrahmanya, C. R. 1996b, ApJS, submitted (Paper II)
Kristian, J. A., Sandage, A. R., & Katem, B. 1974, ApJ, 191, 43
Lacy, M., et al. 1995, MNRAS, 271, 504
Laing, R. A., & Peacock, J. A. 1980, MNRAS, 190, 903

Laing, R. A., Riley, J., & Longair, M. 1983, MNRAS, 204, 151
Landolt, A. 1992, AJ, 103, 340
Large, M. I., Mills, B. Y., Little, A. G., Crawford, D. E., & Sutton, J. M. 1981, MNRAS, 194, 693 (MRC)
Lasker, B. M., Sturch, C. R., McLean, B. J., Russell, J. L., Jenker, H., & Shara, M. M. 1990, AJ, 99, 2019
Lilly, S. J. 1988, ApJ, 333, 161
———. 1989, ApJ, 340, 77
McCarthy, P. 1993, ARA&A, 31, 639
McCarthy, P. J., Kapahi, V. K., van Breugel, W. J. M., & Subrahmanya, C. R. 1990, AJ, 100, 1014
McCarthy, P. J., Persson, S. E., Kapahi, V. K., & van Breugel, W. J. M. 1996a, in preparation (Paper V)
McCarthy, P. J., van Breugel, W. J. M., & Kapahi, V. K. 1996b, in preparation (Paper IV)
McCarthy, P. J., van Breugel, W. J. M., Kapahi, V. K., & Subrahmanya, C. R. 1991, AJ, 102, 522
Owen, F. N., & Keel, W. C. 1995, AJ, 486, 109
Peacock, J. A., & Wall, J. V. 1981, MNRAS, 194, 331
Pearson, T. J., & Readhead, A. C. S. 1981, ApJ, 248, 61
Persson, S. E., West, S. C., Carr, D. M., Sivaramakrishnan, A., & Murphy, D. C. S. 1992, PASP, 104, 204
Rawlings, S. 1994, in ASP Conf. Ser., Vol. 54, Proc. 1st Stromolo Symp., The Physics of Active Galaxies, ed. G. V. Bicknell, M. A. Dopita, & P. J. Quinn (San Francisco: ASP), 253
Rawlings, S., et al. 1996, MNRAS, in press
Rottgering, H., van Ojik, R., & Miley, G. K. 1996, A&A, in press
Saunders, R., Baldwin, J. E., Rawlings, S., Warren, B., & Miller, L. 1989, MNRAS, 238, 777
Spinrad, H., Dey, A., & Graham, J. R. 1995, ApJ, 438, L51
Spinrad, H., Djorgovski, S., Marr, J., & Aguilar L. A. 1985, PASP, 97, 932
Thompson, D. J., & Djorgovski, S. 1994, AJ, 107, 1
Thompson, I., Searle, L., & Krezminski, W. 1996, in preparation
Thuan, T. X., & Gunn, J. E. 1976, PASP, 88, 543
van Ojik, R., Miley, G. K., & Rottgering, H. 1996, A&A, in press
Veron, P. 1966, ApJ, 144, 861
Vigotti, M., Grueff, G., Perley, R. A., Clark, B. G., & Bridle, A. H. 1989, AJ, 98, 419
Wade, R. A., Hoessel, J. G., Elias, J. H., & Huchra, J. P. 1979, PASP, 91, 35
Wall, J. V. 1980, Phil. Trans. R. Soc. Lond., A, 296, 367
Wall, J. V., & Peacock, J. A. 1985, MNRAS, 216, 173
Windhorst, R. A., Koo, D. C., & Kron, R. G. 1985, A&A, 140, 220
Wyndham, J. D. 1966, ApJ, 144, 459
Yates, M. G., Miller, L., & Peacock, J. A. 1989, MNRAS, 240, 129